The *Drosophila* of single-molecule magnetism: $[Mn_{12}O_{12}(O_2CR)_{16}(H_2O)_4]$

Rashmi Bagai and George Christou*

Received 14th July 2008
First published as an Advance Article on the web 23rd February 2009
DOI: 10.1039/b811963e

Single-molecule magnets (SMMs) are individual molecules that can function as nanoscale magnetic particles. The $[Mn_{12}O_{12}(O_2CR)_{16}(H_2O)_4]$ (Mn_{12}; R = Me, Et, *etc.*) family of SMMs was the first one discovered; it is also the one whose study has provided the majority of current knowledge on this interesting magnetic phenomenon, prompting its description here as the *Drosophila* of the field. This *tutorial review* will survey the various chemical studies that have been carried out to date on this family. This will include a discussion of methods that have been developed for their structural and redox transformation, and the effect of the latter on the magnetic and SMM properties.

1. Introduction

Magnets are a multi-billion dollar annual industry with a host of uses such as in switches, computer hard drives, credit/debit/ATM cards, televisions, audio devices, motors, and highly specialized instruments such as medical MRI equipment, among many others. As industry continues the push towards greater miniaturization, smaller devices, and more digital information storage in a computer hard drive or iPod© memory, the need for smaller and smaller magnets increases. Magnetism has consequently become a major sub-division of Nanoscience. The need is for nanoscale magnets of identical size and behaviour, and the standard approach to this has been to make smaller and smaller pieces of traditional magnets, which are composed of metals, metal alloys, metal oxides, or similar. This so-called 'top-down' approach is reaching its limits as the ability to fabricate nanoscale magnets that are of identical size (*i.e.* monodisperse) becomes increasingly more difficult with decreasing size.

The ability of a single molecule to function as a magnet is thus of great importance to the field of nanomagnetism because it represents an alternative, 'bottom-up' route to nanoscale magnetic materials. Indeed, it brings to the area all the advantages of molecular chemistry, including monodispersity, crystallinity, true solubility (rather than colloid formation), protection by a shell of organic groups that prevents close contact of a molecule's magnetic core with those of neighbouring molecules, and the ability to vary this organic shell at will using standard chemical methods.

Such molecules are called single-molecule magnets (SMMs).[1–4] They have also occasionally been called molecular nanomagnets. To function as an SMM, a molecule must display slow magnetization relaxation below a characteristic blocking temperature, T_B. This behaviour results from a large ground spin state (S) (*i.e.*, lots of unpaired electrons) combined with a large and negative Ising (or easy-axis) type of magnetoanisotropy, as measured by the axial zero-field

Department of Chemistry, University of Florida, Gainesville, Florida 32611-7200, USA. E-mail: christou@chem.ufl.edu

Rashmi Bagai

Rashmi Bagai received her MSc degree in Chemistry from the Indian Institute of Technology, Delhi in 2000. After working there as a CSIR research fellow for two years, she started doctoral research in the Christou group at the University of Florida. During this period, she received a Harry H. Sisler Fellowship, a Proctor & Gamble Talent Award, and a Crow Award. She received her PhD in May 2008.

George Christou

George Christou received his PhD in Chemistry from Exeter University, and was a Postdoctoral Fellow at Manchester and a NATO Fellow at Stanford and Harvard Universities. He became a lecturer at Imperial College, before moving to Indiana University in 1983. In 2001 he took up the Drago Chair of Chemistry at the University of Florida. His research is in the synthesis and physical-inorganic chemistry of 3d metal clusters of various nuclearities, and their relevance to bioinorganic chemistry and magnetic materials.

splitting (zfs) parameter, D. This combination leads to a significant barrier to magnetization reversal, whose upper limit (U) is given by $S^2|D|$ or $(S^2 - 1/4)|D|$ for integer and half-integer spins, respectively. Note that intermolecular interactions must be minimal, and thus merely represent perturbations of single-molecule behaviour, otherwise 1-, 2- or 3-D molecule-based magnetism is observed. Experimentally, an SMM exhibits the superparamagnet-like properties typical of much larger nanoscale pieces of traditional magnets, displaying both a frequency-dependent out-of-phase ac magnetic susceptibility signal, and hysteresis in a plot of magnetization *versus* applied dc magnetic field; these are both classical properties of magnetic materials. In addition, they are true 'mesoscale' particles, clearly straddling the classical/quantum boundary, and thus display not just classical properties but also quantum properties such as quantum tunnelling of the magnetization vector (QTM) through the barrier.[5] For all these reasons, SMMs have been proposed for various specialized applications, such as ultra-high density memory devices, spintronics, and quantum computing.[6,7]

Although complexes displaying SMM behaviour are known for several metals, manganese cluster chemistry containing at least some Mn^{III} atoms has been the most fruitful source to date.[3,4,8] Using only a limited assortment of ligands and starting materials, cluster products with a wide range of Mn_x nuclearities can be obtained, with x taking almost all values up to 30, plus Mn_{32}, Mn_{40}, Mn_{70} and Mn_{84}, the latter being the largest to date.[8] The first SMM to be identified was $[Mn_{12}O_{12}(O_2CMe)_{16}(H_2O)_4]$ (**1**; $Mn^{III}{}_8Mn^{IV}{}_4$),[2,9] whose synthesis and preliminary magnetic properties were first reported by Lis as long ago as 1980,[10] and **1** remains the most widely investigated SMM (Fig. 1). Its ease of preparation, crystallinity, high S and D values, and high molecular (S_4) and space group ($I\bar{4}$) symmetry, which simplifies the spin Hamiltonian by precluding second-order transverse (rhombic) terms, have made **1** and other subsequent members of the $[Mn_{12}O_{12}(O_2CR)_{16}(H_2O)_4]$ (R = Et, Ph, *etc.*) family the favourites within both the chemistry and physics communities for detailed study by a myriad of techniques. Thus, in the same way that the study of the *Drosophila* genus of flies has been the source of so much of our current knowledge of genetics, so has the study of the $[Mn_{12}O_{12}(O_2CR)_{16}(H_2O)_4]$ family been the source of so much of what is currently known about single-molecule magnetism, prompting us to call it the *Drosophila* of the field in the title of this review.

Interesting as compound **1** may be, there is only a limited amount of knowledge that can be extracted from a single datum point. It was thus clear right from the outset that a deep and broad understanding of this field could only come from a systematic study of a family of Mn_{12} SMMs that had been modified in various directed ways. As a result, an arsenal of methods has since been systematically developed by our group for modifying the Mn_{12} family of SMMs in a variety of targeted and controllable ways. The central inorganic Mn/O core of these molecules is contained within a shell of organic ligands, and one type of methodology that was successfully developed many years ago was the modification of this organic periphery *via* ligand substitution reactions on preformed materials.[9,11] Indeed, the systematic variation of the size and

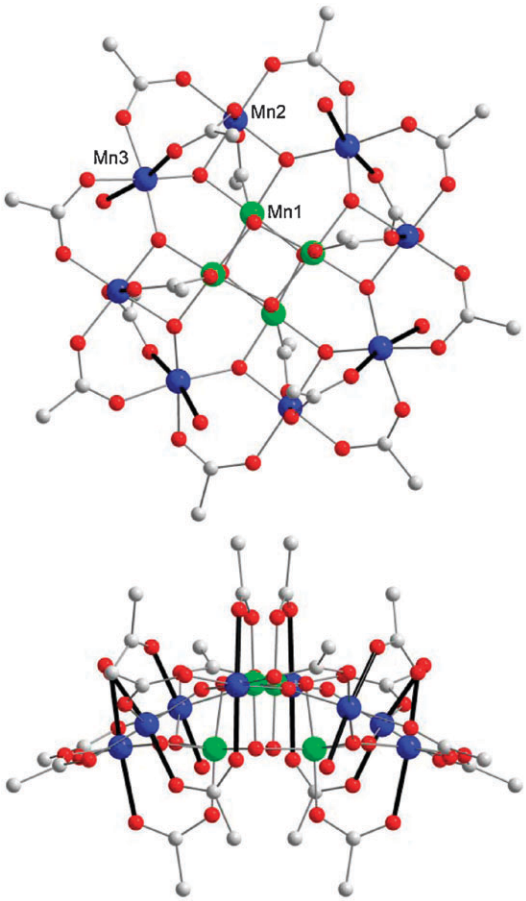

Fig. 1 Structure of complex **1** viewed along the crystal c-axis (top) and b-axis (bottom). The thicker black bonds indicate the positions of the Mn^{III} Jahn–Teller elongation axes. Colour scheme: Mn^{IV} green, Mn^{III} blue, O red, C grey.

electronic properties of the carboxylates has proved invaluable as a means by which the structural, spectroscopic and magnetic properties can be investigated and interpreted in a comparative manner. This variation has also permitted the tuning of the solubilities, redox potentials, and magnetic properties of the molecules. A distinctly different type of modification of Mn_{12} complexes has been their generation and study at different oxidation levels to assess the influence of the electron count on various properties. A further but more subtle way of modifying the molecules is to grow the crystals from various solvents, which can lead to variations in the space group and precise solvent content of the crystals, and which in turn lead to variations in the local site-symmetry and environment around the molecules. While this latter modification might seem likely to lead to insignificant changes to the properties of the molecule, it has on the contrary been found to lead to surprisingly large changes. Because of all these controlled modifications, current knowledge and understanding of the properties of Mn_{12} SMMs, and by extension of all SMMs, have been greatly advanced. We shall herein review these studies of the Mn_{12} family, concentrating on the chemistry of this area as is appropriate for a chemistry journal; reviews of SMMs in general are available elsewhere,[4,8]

which include brief discussions of the Mn_{12} family. These modification methods have also proved to be the *sine qua non* of most of the attempts to form 2-D and other arrays of Mn_{12} molecules on selected surfaces, such as gold and other surfaces, and Langmuir–Blodgett (LB) and polymer films.[12] These have met with mixed success to date, but in any case fall outside the scope of this review and will not be further discussed.

2. Preparation of $[Mn_{12}O_{12}(O_2CR)_{16}(H_2O)_4]$

This section will describe the various procedures that have been developed for the synthesis of Mn_{12} complexes and their controlled modification in a number of ways. These procedures are summarized for convenience in Scheme 1.

2.1 Direct synthesis

The procedure reported by Lis in 1980 for the preparation of $\mathbf{1}\cdot 2MeCO_2H\cdot 4H_2O$,[10] and small modifications thereof,[9] is a very convenient one that allows ready access to high yields of crystalline material. The preparation involves the comproportionation reaction of $Mn(O_2CMe)_2$ and $KMnO_4$ in 60% aq. acetic acid in a ratio appropriate for the final +3.33 average Mn oxidation level (eqn (1)).

$$44Mn^{2+} + 16Mn^{7+} \rightarrow 5Mn^{3+}{}_8Mn^{4+}{}_4 \qquad (1)$$

Compound **1** can also be prepared by the oxidation of $[Mn_3O(O_2CMe)_6(py)_3](ClO_4)$ (py is pyridine) by $KMnO_4$ in 60% aq. acetic acid.[9] This procedure is high yield but requires prior formation of the trinuclear complex and has thus not been employed on a regular basis. Similarly, $[Mn_{12}O_{12}(O_2CPh)_{16}(H_2O)_4]$ can be obtained by comproportionation of $NBu^n_4MnO_4$ with $Mn(O_2CMe)_2$ in the presence of benzoic acid,[9] and $[Mn_{12}O_{12}(O_2CC_6H_4\text{-}p\text{-}R)_{16}(H_2O)_4]$ (R = Cl, Me, Bu^t) by the analogous reaction of $Mn(ClO_4)_2$ and $NBu^n_4MnO_4$ in ethanol in the presence of R-*p*-$C_6H_4CO_2H$; the yields of these derivatives are generally less than those obtained by carboxylate substitution (*vide infra*). A modified version of **1**, $[Mn_{12}O_{12}(O_2CMe)_{16}(MeOH)_4]$, can be made by reaction of $Mn(O_2CMe)_2$ with $NBu^n_4MnO_4$ in MeOH : $MeCO_2H$ (3 : 2 v/v).[13] The analogous complex, $[Mn_{12}O_{12}(O_2CCH_2Bu^t)_{16}(MeOH)_4]$ has been synthesized by recrystallization of $[Mn_{12}O_{12}(O_2CCH_2Bu^t)_{16}(H_2O)_4]$ from $MeOH/Et_2O$.[14]

2.2 Carboxylate substitution

One of the first reactivity characteristics of Mn_{12} to be established was its ability to undergo carboxylate substitution reactions (Scheme 1).[9,11] This provided an extremely useful and convenient means of accessing other carboxylate derivatives of **1**, which proved invaluable for a number of reasons, including increased solubility in organic solvents compared to **1**. This ligand substitution reaction (eqn (2)) is an equilibrium that must be driven to completion by (i) multiple treatments employing an excess of an RCO_2H that is more acidic than $MeCO_2H$; and/or (ii) removal of $MeCO_2H$ as its toluene azeotrope to drive the equilibrium of eqn (2) to the right. These procedures will reliably give pure product in high yields for numerous carboxylate types.[15] Method (ii) is particularly useful for incorporating carboxylate groups whose conjugate acid has a pK_a comparable to, or even higher than that of acetic acid. Note that the starting material for the carboxylate substitution need not be complex **1**.

$$[Mn_{12}O_{12}(O_2CMe)_{16}(H_2O)_4] + 16RCO_2H \rightleftharpoons (16-x)MeCO_2H + [Mn_{12}O_{12}(O_2CMe)_x(O_2CR)_{16-x}(H_2O)_4] \qquad (2)$$

Carboxylate substitution has found widespread utility in Mn_{12} chemistry: for example, Gerbier *et al*. used this method with (1-[*N*-*t*-butyl-*N*-(oxyl)amino]-4-benzoic acid radical to introduce spin-carrying carboxylate groups onto the Mn_{12} molecule, where they were found to couple antiferromagnetically to the $[Mn_{12}O_{12}]$ core;[16] Coronado *et al*. have synthesized Mn_{12} derivatives bearing cationic carboxylate groups that can interact with paramagnetic or redox active anions in order to study their effect on the magnetic properties;[17a] Veciana *et al*. have prepared a biphenyl-carboxylate derivative to investigate Mn_{12} molecules or monolayers on surfaces;[17b] Park and Jung have prepared a strongly hydrophobic Mn_{12} derivative by replacement of acetate with stearate groups;[18] Zhao *et al*. have prepared the $CF_3CO_2^-$ derivative as a potentially better candidate for incorporation of Mn_{12} into films since $CF_3CO_2^-$ is known to render compounds highly soluble and more volatile;[19] Bian *et al*. have prepared naphthalene-carboxylate derivatives that assemble two-dimensionally *via* π–π interactions;[20] Willemin *et al*. have made methacrylate derivatives to prepare chemically and thermally stable nanocomposites;[21] several groups have employed sulfur-based carboxylate derivatives in attempts to deposit Mn_{12} molecules onto gold

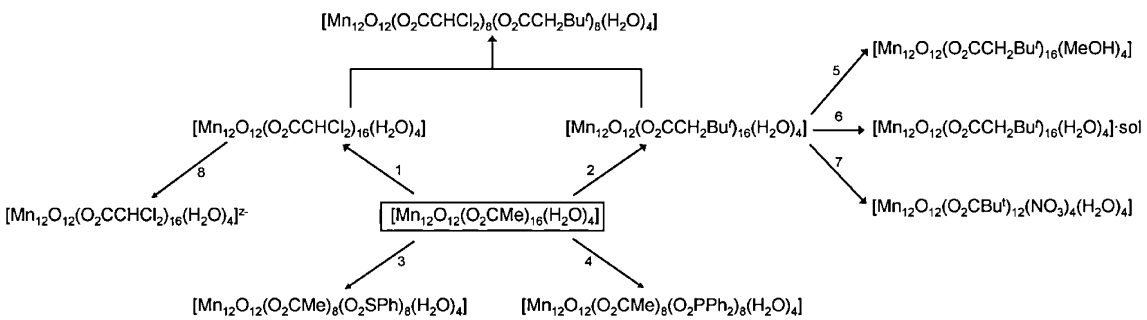

Scheme 1 The established transformations of $[Mn_{12}O_{12}(O_2CMe)_{16}(H_2O)_4]$. Procedures. *Via* acetic acid/toluene azeotrope removal: 1, $CHCl_2CO_2H$; 2, $Bu^tCH_2CO_2H$; 3, $PhSO_3H$; 4, Ph_2PO_2H. By recrystallization: 5, $MeOH/Et_2O$ (high-symmetry); 6, $CH_2Cl_2/MeNO_2$ (LT), $CH_2Cl_2/MeCN$ (HT). Acidolysis: 7, HNO_3. Chemical Reduction: 8, addition of z (z = 1, 2 or 3) equiv of PPh_4I/NR_4I (R = Me, Et, *etc*.).

surfaces;[12,22,23] and Heersche *et al.*, and others since, have used the same approach to insert single Mn_{12} molecules between gold nano-electrodes.[24]

2.3 Site-selective substitution

As emphasized in Fig. 1 and discussed further in section 3, the eight Mn^{III} Jahn–Teller (JT) elongation axes in Mn_{12} are all axial with respect to the disk-like molecule. This has allowed site-selective substitution reactions to be developed, based on the enhanced reactivity to electrophiles of carboxylate groups lying on the JT axes. Of the 16 carboxylates, four (type **A**) have both their O atoms on JT axes, four (type **B**) have one, and eight (type **C**) have none because they are equatorial. Since a lengthening (weakening) of a Mn–O bond will increase the nucleophilicity of the O atom, the relative susceptibility of the carboxylate groups to electrophilic attack would be expected to be **A** > **B** > **C**, and this has proved to be the case. The resulting selectivity has allowed a variety of asymmetric Mn_{12} derivatives to be prepared.

Site-selective abstraction of the four type **A** carboxylate groups of $[Mn_{12}O_{12}(O_2CR)_{16}(H_2O)_4]$ (R = CH_2Bu^t, Ph) has been achieved by protonation with four equivalents of HNO_3 in MeCN, cleanly giving $[Mn_{12}O_{12}(O_2CR)_{12}(NO_3)_4(H_2O)_4]$ (eqn (3)).[25] The four nitrate groups are bound in the same η^1:η^1:μ bridging modes as the displaced carboxylate groups had been at the type **A** axial positions.

$$[Mn_{12}O_{12}(O_2CR)_{16}(H_2O)_4] + 4HNO_3 \rightarrow [Mn_{12}O_{12}(O_2CR)_{12}(NO_3)_4(H_2O)_4] + 4RCO_2H \quad (3)$$

The same strategy has allowed a related site-selectivity involving mixed-carboxylate ligation to be developed. The hypothesis was that the more basic carboxylate groups would thermodynamically favour binding at the non-JT equatorial (type **C**) sites where they can form the strongest Mn–O bonds, *i.e.* bond energies can be maximized increasing the thermodynamic stability of the whole molecule. This has been beautifully confirmed by the mixed-carboxylate complexes $[Mn_{12}O_{12}(O_2CCHCl_2)_8(O_2CCH_2Bu^t)_8(H_2O)_4]$ and $[Mn_{12}O_{12}(O_2CCHCl_2)_8(O_2CEt)_8(H_2O)_4]$, prepared either by the 1 : 1 reaction of the corresponding homo-carboxylate species (eqn (4)) or the reaction of $[Mn_{12}O_{12}(O_2CR)_{16}(H_2O)_4]$ with eight equivalents of $R'CO_2H$.[26] The resulting 8 : 8 product complexes both have the less basic $CHCl_2CO_2^-$ ligands in the axial positions and the more basic ones (R′ = CH_2Bu^t or Et) in the equatorial ones; the relative basicities are $Bu^tCH_2CO_2^-$ > $EtCO_2^-$ ≫ $CHCl_2CO_2^-$. It was proposed that this methodology could form the basis of regioselective introduction of groups for subsequent binding of Mn_{12} to surfaces (as well as other applications) and this approach was indeed subsequently used by Pacchioni *et al.* to add two S-containing dicarboxylate groups at the four type **A** and **B** positions for attempts to bind Mn_{12} to a Au surface.[23]

$$[Mn_{12}O_{12}(O_2CR)_{16}(H_2O)_4] + [Mn_{12}O_{12}(O_2CR')_{16}(H_2O)_4] \rightarrow 2[Mn_{12}O_{12}(O_2CR)_8(O_2CR')_8(H_2O)_4] \quad (4)$$

2.4 Non-carboxylate substitution

In a manner analogous to carboxylate substitution, Mn_{12} complexes have also been derivatized in a site-specific fashion with non-carboxylate ligands other than nitrate. One objective has been to replace just the eight axial, or just the eight equatorial carboxylate groups with non-carboxylate groups, and thus obtain a mixed-ligand derivative with the two types of ligands in specific positions on the Mn_{12} molecule. Indeed, the reaction of **1** with 8 equiv. of benzenesulfonic acid gives $[Mn_{12}O_{12}(O_2CMe)_8(O_3SPh)_8(H_2O)_4]$ with the $PhSO_3^-$ groups at the eight axial (**A** and **B**) sites above and below the disk-like $[Mn_{12}O_{12}]$ core, again as expected on the basis of relative basicities.[27] In contrast, expansion of the Mn_{12} family into P-containing ligands by ligand substitution reactions employing diphenylphosphinic acid (Ph_2PO_2H) did successfully yield the 8 : 8 complex $[Mn_{12}O_{12}(O_2CMe)_8(O_2PPh_2)_8(H_2O)_4]$, but the large steric bulk of the $Ph_2PO_2^-$ groups resulted in their equal distribution between axial and equatorial sites, *i.e.* steric effects overcame the basicity effects.[28] However, when only four similarly bulky $(PhO)_2PO_2^-$ groups were introduced by Kuroda-Sowa *et al.*, steric effects were lessened and the product $[Mn_{12}O_{12}(O_2CPh)_{12}(O_2P(OPh)_2)_4(H_2O)_4]$ did now have the non-carboxylates in axial positions.[29] Similarly for $[Mn_{12}O_{12}(O_2CMe)_{12}(O_3SMe)_4(H_2O)_3]$[30] and the interesting $[Mn_{12}O_{12}(O_2CMe)_{12}(O_2P(OPh)_2)_4]$ that also contains four five-coordinate Mn^{III} atoms, *i.e.* no bound water molecules.[31]

It should be noted with reference to the magnetic properties of Mn_{12} complexes to be discussed below that all the mixed-carboxylate, and non-carboxylate-containing complexes discussed in this section possess S, D, g and U_{eff} values within the normal range for Mn_{12} carboxylate complexes. Thus, the altered ligation does not have a significant effect on the electronic properties of the core or the resulting magnetic properties.

3. Structure of $[Mn_{12}O_{12}(O_2CR)_{16}(H_2O)_4]$

The $[Mn_{12}O_{12}(O_2CR)_{16}(H_2O)_4]$ complexes contain a central $Mn^{IV}{}_4O_4$ cubane held within a nonplanar ring of eight Mn^{III} ions by eight μ_3-O^{2-} ions (Fig. 1, top). Peripheral ligation is provided by 16 bridging carboxylate groups and 4 (sometimes fewer) terminal water molecules. The eight outer Mn^{III} atoms divide by symmetry into two groups of four: in group I, each Mn^{III} is bridged to a single Mn^{IV} by two μ_3-O^{2-} ions (Mn2 of Fig. 1), whereas in group II, each Mn^{III} is bridged to two Mn^{IV} ions by two μ_3-O^{2-} bridges (Mn3). The four central Mn^{IV} atoms are thus group III. The four water molecules are bound only to Mn^{III} atoms in group II, one to each Mn^{III} atom in **1** giving the 1 : 1 : 1 : 1 (S_4) isomer. The exact number and disposition of the water molecules can vary from one Mn_{12} to another. For example, $[Mn_{12}O_{12}(O_2CEt)_{16}(H_2O)_3]$ has only three water ligands in a 1 : 1 : 1 fashion, with one group II Mn^{III} thus five coordinate. Similarly, the four waters in $[Mn_{12}O_{12}(O_2CPh)_{16}(H_2O)_4]$ are arranged in a 2:0:2 (D_2) fashion.[9] Also, 1 : 2 : 1, 1 : 1 : 2 and 2 : 0 : 1 isomers have been seen in different Mn_{12} molecules,[9,11,19,32,33] as well as the $[Mn_{12}O_{12}(O_2CMe)_{12}(O_2P(OPh)_2)_4]$ complex already mentioned with no waters at all.[31]

As expected for high-spin (d^4) Mn^{III} in near-octahedral geometry, there is a first-order Jahn–Teller (JT) distortion, which almost always takes the form of an axial elongation of two *trans* bonds, typically by 0.1–0.2 Å. These JT elongation

axes avoid the Mn–O^{2-} bonds, the shortest and strongest in the molecule, and thus they are all axially disposed, roughly perpendicular to the $[Mn_{12}O_{12}]$ disk-like core (Fig. 1, bottom). As a result, there is a near-parallel alignment of the eight Mn^{III} JT axes along the molecular *z*-axis, and this is the origin of the significant magnetic anisotropy (*D* value) of the easy-axis type that so greatly influences the observed magnetic properties (*vide infra*).

The structures of some Mn_{12} complexes appear typical at first glance but closer examination reveals that one Mn^{III} JT elongation axis is abnormally oriented, equatorially rather than axially, and thus contains an oxide ion. Examples of such complexes include $[Mn_{12}O_{12}(O_2CC_6H_4\text{-}p\text{-}Me)_{16}(H_2O)_4]\cdot Me\text{-}p\text{-}C_6H_4CO_2H$, and $[Mn_{12}O_{12}(O_2CCH_2Bu^t)_{16}(H_2O)_4]\cdot CH_2Cl_2\cdot MeNO_2$.[32,34,35] The abnormal JT axis in the latter is shown in Fig. 2 as being on atom Mn6. As the crystals lose solvent on drying, the abnormal JT axis converts to a normal orientation. Similarly, recrystallization from CH_2Cl_2/MeCN gives $[Mn_{12}O_{12}(O_2CCH_2Bu^t)_{16}(H_2O)_4]\cdot CH_2Cl_2\cdot MeCN$, in which all JT axes have a normal orientation.[35] These results show that the abnormal orientation is a local higher-energy situation stabilized by subtle crystal packing effects, and reorients to the preferred situation if the latter are relaxed. The ability of a molecule to exist in two distinct forms differing only in the relative orientation of one or more JT axes has been named by us as 'Jahn–Teller isomerism'. Its importance extends beyond mere structural aspects, for it significantly affects the magnetic properties of Mn_{12} molecules (*vide infra*).

Some additional comments about the structure of $\mathbf{1}\cdot 2MeCO_2H\cdot 4H_2O$ are pertinent. It has become the most widely studied SMM, not only because it was first to be recognized as an SMM but also because of its high symmetry, as mentioned earlier. However, it has relatively recently become apparent that **1** is far from being the 'ideal' Mn_{12} to study, owing to complications arising from the solvent of crystallization. Specifically, each Mn_{12} is surrounded by four acetic acid molecules, with each of the latter lying symmetrically between that Mn_{12} and a neighbouring one. Each acetic acid can form an OH···O hydrogen-bond with an acetate ligand on one (and only one) of the two Mn_{12} that it lies between. Therefore, each Mn_{12} molecule is hydrogen-bonded to *n* (*n* = 0–4) of the four

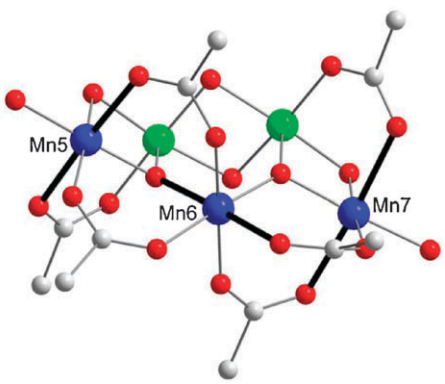

Fig. 2 Portion of the structure of $[Mn_{12}O_{12}(O_2CCH_2Bu^t)_{16}(H_2O)_4]\cdot CH_2Cl_2\cdot MeNO_2$ showing normal disposition of JT elongation axes on Mn5 and Mn7, but an abnormal one containing an oxide ion on Mn6. Colour scheme: Mn^{IV} green, Mn^{III} blue, O red, C grey.

acetic acid molecules around it.[10,36] Of the six resulting isomers (there are both *cis* and *trans* possibilities for *n* = 2), only with *n* = 0 and *n* = 4 does the Mn_{12} molecule retain S_4 (axial) symmetry, the other four isomers having lower (rhombic) symmetry. This would not be of serious consequence except that this distribution of isomers exhibits a significant distribution in the resulting magnetic properties. Thus, $\mathbf{1}\cdot 2MeCO_2H\cdot 4H_2O$ is not the paragon of the Mn_{12} family for detailed study using models that assume axial symmetry in the spin Hamiltonian.

Single-environment, high-symmetry Mn_{12} complexes have recently become available, however. $[Mn_{12}O_{12}(O_2CCH_2Br)_{16}(H_2O)_4]\cdot 4CH_2Cl_2$ (space group $I4_1/a$) was reported in 2001,[37] prepared by ligand substitution on **1**. Each Mn_{12} molecule is surrounded by four CH_2Cl_2 molecules that exhibit insignificant contacts with the Mn_{12} periphery, and the crystal is thus 'clean', *i.e.* essentially a single molecular environment. The latter became dramatically obvious in subsequent extensive studies of the properties of this complex using micro-SQUID, high-frequency EPR (HFEPR) and ^{55}Mn NMR techniques, in all cases using single crystals.[14,38–41] All measurements gave far superior quality data than previously obtained from $\mathbf{1}\cdot 2MeCO_2H\cdot 4H_2O$. The lower inhomogeneous broadening of EPR and NMR spectral lines not only allows for higher precision data, but also extraction of additional information previously unavailable, such as quadrupolar coupling parameters from the quadrupolar splitting seen in the ^{55}Mn NMR spectra due to the ^{55}Mn (*I* = 5/2) nucleus (*vide infra*).

Another high symmetry Mn_{12} complex has recently been obtained, $[Mn_{12}O_{12}(O_2CCH_2Bu^t)_{16}(MeOH)_4]\cdot MeOH$,[14] which crystallizes in space group $I\bar{4}$. There is only one MeOH molecule of crystallization, which sits on an S_4 symmetry axis and also does not cause a range of Mn_{12} molecular environments. Furthermore, the bulky $Bu^tCH_2CO_2^-$ groups more efficiently separate the clusters from their neighbours, minimizing inter-cluster dipolar interactions. As a result, this Mn_{12} has proven invaluable not only for HFEPR and ^{55}Mn NMR studies as mentioned above, but also for detailed QTM studies that have provided high resolution data far superior to those previously available for $\mathbf{1}\cdot 2MeCO_2H\cdot 4H_2O$. This has permitted an unprecedented level of analysis of the data to be accomplished.[42,43] It may even allow in the future the identification and study of particularly subtle and difficult to detect magnetic phenomena such as quantum interference effects caused by higher-order (>2nd-order) transverse terms in the spin Hamiltonian. Overall, these studies using $[Mn_{12}O_{12}(O_2CCH_2Br)_{16}(H_2O)_4]\cdot 4CH_2Cl_2$ and $[Mn_{12}O_{12}(O_2CCH_2Bu^t)_{16}(MeOH)_4]\cdot MeOH$ have finally allowed the ideal properties of the Mn_{12} SMMs in truly high symmetry to be observed. As the saying goes, 'one doesn't know what one is missing until one finds it'!

4. Properties of $[Mn_{12}O_{12}(O_2CR)_{16}(H_2O)_4]$

4.1 Electrochemistry

Extensive electrochemical studies on the $[Mn_{12}O_{12}(O_2CR)_{16}(H_2O)_4]$ family have revealed a rich redox chemistry involving several oxidation and reduction processes (Table 1). Several of the

latter are reversible by the usual electrochemical criteria (peak separations in cyclic voltammetry (CV); peak broadness in differential pulse voltammetry (DPV); $i_{anodic}/i_{cathodic}$ peak current ratio, and proportionality of peak current to the square root of the scan rate),[9,11] suggesting that the Mn_{12} complexes are stable in multiple oxidation levels. The CV and DPV scans for the R = $CHCl_2$ Mn_{12} are shown is Fig. 3. In addition, and as expected, the redox processes are very sensitive to the electron-withdrawing or -donating ability of the carboxylate R group. The $E_{1/2}$ values (*vs.* ferrocene) in Table 1 for the first one-electron reduction (E_3) range from +0.91 V for R = $CHCl_2$ to 0.00 V for the R = C_6H_4-*p*-OMe, a massive range of almost a volt. Similarly, the second reduction ranges from +0.61 V for R = $CHCl_2$ to −0.50 V for R = Et. This ability to tune the redox potentials over such a large range has been invaluable for our subsequent attempts to isolate and study Mn_{12} complexes in other oxidation levels to assess the resulting change in the magnetic properties.

All success to date has been on the reducing side, where one-, two-, and recently three-electron reduced $[Mn_{12}]^{z-}$ (z = 1–3) derivatives have been generated, isolated, crystallized and studied by various methods. Electron-withdrawing R groups have been favoured for this work, since they reduce the electron density in the core and make multiple reductions thermodynamically more accessible to the preferred reductant, iodide.[11,44] The latter was chosen because of its sufficient yet mild reducing strength, its ready availability as a variety of salts of organic cations, the high solubility of many of the latter in organic solvents, and the ease of removal of the only by-product, elemental I_2 (eqn (5)).

$$Mn_{12} + zI^- \rightarrow [Mn_{12}]^{z-} + (z/2)I_2 \qquad (5)$$

The first reduced Mn_{12} was obtained by one-electron reduction of $[Mn_{12}O_{12}(O_2CEt)_{16}(H_2O)_3]$ with PPh_4I leading to isolation of $(PPh_4)[Mn_{12}O_{12}(O_2CEt)_{16}(H_2O)_4]$.[11] Since then, both one- and two-electron reductions have been accomplished for Mn_{12} complexes with carboxylate ligands bearing the strongly electron-withdrawing R = $CHCl_2$ or C_6F_5 groups, giving $(PPh_4)_z[Mn_{12}O_{12}(O_2CCHCl_2)_{16}(H_2O)_4]$[44] and $(NMe_4)_z[Mn_{12}O_{12}(O_2CC_6F_5)_{16}(H_2O)_4]$ (z = 1 or 2).[15]

Table 1 Electrochemical data for $[Mn_{12}O_{12}(O_2CR)_{16}(H_2O)_4]$ complexes[a]

R	E_1/V[b]	E_2/V[c]	E_3/V[d]	E_4/V[e]
CH_3[f]	p.r.	0.82	0.19	−0.07
CH_2CH_3	1.03	0.79	0.02	−0.50
C_6H_5	1.16	0.82	0.12	−0.23
$C_6H_4OCH_3$	1.00	0.70	0.00	p.r.
$C_6H_4C_6H_5$	1.12	0.79	0.10	p.r.
C_6H_4F	1.18	0.93	0.23	−0.10
C_6H_4Cl	1.22	0.97	0.30	−0.03
$C_6H_4NO_2$	n.o.	1.05	0.47	0.22
C_6H_3-2,4-$(NO_2)_2$	—	n.o.	0.74	0.45
C_6F_5	—	n.o.	0.64	0.30
CH_2Cl[f]	—	n.o.	0.60	0.30
$CHCl_2$[f]	—	n.o.	0.91	0.61

[a] In CH_2Cl_2, unless otherwise indicated; values are DPV peak potentials *vs.* ferrocene. [b] 2nd oxidation. [c] 1st oxidation. [d] 1st reduction. [e] 2nd reduction. [f] In MeCN. p.r. = poorly resolved; n.o. = not observed.

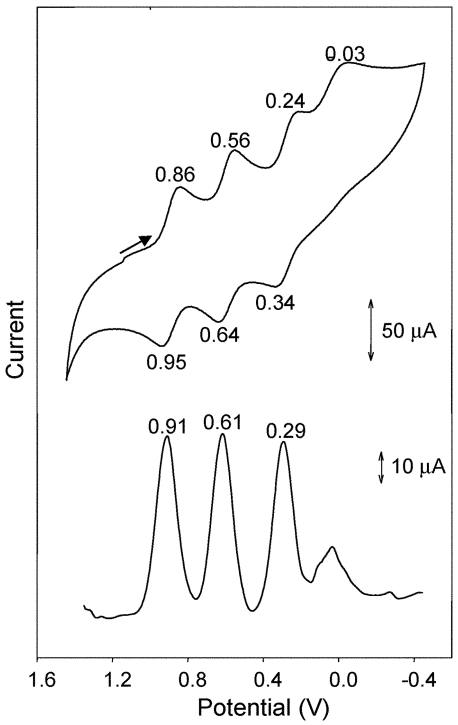

Fig. 3 CV at 100 mV s^{-1} (top) and DPV at 20 mV s^{-1} (bottom) for $[Mn_{12}O_{12}(O_2CCHCl_2)_{16}(H_2O)_4]$ in MeCN containing 0.1 M NBu_4PF_6 as supporting electrolyte. The indicated potentials are *vs.* ferrocene. Reprinted with permission from ref. 44. Copyright 2003 American Chemical Society.

The CV and DPV of $[Mn_{12}O_{12}(O_2CCHCl_2)_{16}(H_2O)_4]$ (Fig. 3) also exhibit a third reversible reduction accessible to I^-, and indeed the three-electron reduced complex $[Mn_{12}O_{12}(O_2CCHCl_2)_{16}(H_2O)_4]^{3-}$ was more recently isolated and studied as its NPr_4^+ and NMe_4^+ salts.[45]

In addition to $[Mn_{12}]^-$ salts with diamagnetic cations, there are also $[Mn_{12}]^-$ salts whose cation is an organic radical cation such as *m*-*N*-methylpyridinium nitronyl nitroxide or a paramagnetic metallocenium cation such as ferrocenium. These were prepared in order to probe any effect of the cation spin on the magnetic properties of the anion.[46]

Structure of $[Mn_{12}]^{z-}$ complexes (z = 1–3). An immediate and very important structural question about the $[Mn_{12}]^{z-}$ (z = 1–3) complexes was where do the added electrons go? The successful attainment of the crystal structures of various $[Mn_{12}]^-$ and $[Mn_{12}]^{2-}$ complexes has established that the electrons localize on Mn^{III} atoms of the outer ring rather than on Mn^{IV} atoms of the inner cubane.[11,15,44] Shown in Fig. 4 are the resulting distributions of Mn oxidation states in the complexes. The one and two added electrons in $[Mn_{12}]^-$ and $[Mn_{12}]^{2-}$ add to Mn^{III} atoms of group II converting them to Mn^{II}, giving a $Mn^{IV}{}_4Mn^{III}{}_7Mn^{II}$ and $Mn^{IV}{}_4Mn^{III}{}_6Mn^{II}{}_2$ oxidation state description, respectively. The $[Mn_{12}]^{3-}$ anion is insufficiently stable in solution to permit suitable single-crystals to be grown for crystallography, but on the basis of the $[Mn_{12}]^-$ and $[Mn_{12}]^{2-}$ structures, and the magnetic properties of the $[Mn_{12}]^{z-}$ (z = 0–3) series, it is clear that the third added electron also adds to a formerly Mn^{III} atom of

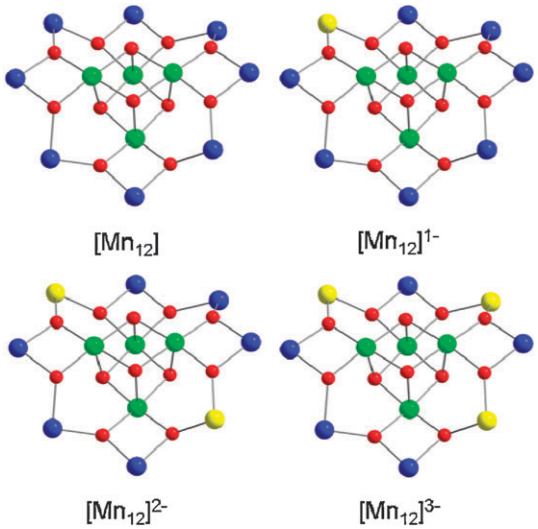

Fig. 4 $[Mn_{12}O_{12}]$ cores of neutral Mn_{12}, and one, two and three electron reduced Mn_{12} complexes. Colour scheme: Mn^{IV} green, Mn^{III} blue, Mn^{II} yellow, O red.

group II giving a $Mn^{IV}{}_4Mn^{III}{}_5Mn^{II}{}_3$ situation. Note that in all cases the electrons are valence-trapped, in the solid state at least.

The counter-intuitive reduction of Mn^{III} rather than Mn^{IV} can be assigned to the very different environments these metals are in within the Mn_{12} core: (i) The Mn^{IV} atoms are each bound to five hard O^{2-} ions, which favour higher oxidation states and would thus disfavour reduction to Mn^{III}; and (ii) reduction of Mn^{IV} would generate a Mn^{III} whose JT distortion would have to include at least one Mn-oxide bond and would introduce strain into the relatively rigid $[Mn_4O_4]$ cubane. In contrast, reduction of an outer Mn^{III} can occur with little perturbation of the basic $[Mn_{12}O_{12}]$ structure. Together, these factors rationalize the thermodynamic preference for reduction of Mn^{III} to Mn^{II}.

4.2 NMR spectroscopy

True solubility (rather than colloid formation) in organic solvents is a major advantage of SMMs over traditional magnetic nanoparticles, but only if their structure remains unchanged on dissolution. A variety of NMR studies (^1H, ^{19}F, *etc.*) on Mn_{12} complexes have therefore been carried out over the years in order to probe their structures in solution.[11,15] Mn^{III} is generally amenable to NMR spectroscopic study because it has a relatively fast electron relaxation time and thus the latter cannot facilitate nuclear relaxation as efficiently as, for example, Mn^{II}. The spectra of various substituted Mn_{12} complexes show that they retain their structural integrity upon dissolution in CD_2Cl_2 or CD_3CN. The S_4 symmetry of **1** in the solid state indicates four types of carboxylates by symmetry in a 1 : 1 : 1 : 1 ratio, two axial (types **A** and **B**) and two equatorial (two symmetry inequivalent sets within type **C**). In fact, the ^1H NMR spectrum of a CD_3CN solution of **1** at room temperature exhibits only three paramagnetically-shifted acetate peaks at δ = 13.9, 41.8 and 48.2 ppm, but in a 1 : 2 : 1 integration ratio, and a significantly broader signal at 18.7 ppm due to a weighted average of rapidly exchanging bound and solvent H_2O molecules.[11] The spectra of many other Mn_{12} complexes show the same 1 : 2 : 1 pattern, showing that it is not just due to a coincidental superposition of two of the peaks. The solution spectrum is thus consistent with effective D_{2d} symmetry, under which all the equatorial (type **C**) acetates are equivalent. Extensive variable-temperature studies of various Mn_{12} complexes have established that a fluxional process is occurring that involves exchange of the axial water molecules and one of the type **A** carboxylate groups; the fluxionality is fast on the NMR timescale at room temperature and serves to introduce vertical (dihedral) mirror planes onto the molecule.[25] This makes the two sub-types of equatorial carboxylates equivalent, and the effective solution symmetry thus becomes D_{2d} rather than S_4. This gives the 1 : 2 : 1 spectral pattern: (a) four type **B** axial carboxylates bridging $Mn^{IV}\cdots Mn^{III}$ pairs, (b) eight type **C** equatorial carboxylates bridging $Mn^{III}\cdots Mn^{III}$ pairs, and (c) four axial type **A** carboxylates bridging $Mn^{III}\cdots Mn^{III}$ pairs.

The ^1H and ^{19}F NMR spectra have also been obtained for $[Mn_{12}]^{1-}$ and $[Mn_{12}]^{2-}$ complexes to probe their behaviour in solution. The ^1H NMR spectra of the $[Mn_{12}O_{12}(O_2CHCl_2)_{16}(H_2O)_4]^{z-}$ (z = 0–2) family in CD_2Cl_2 solution are shown in Fig. 5. The neutral Mn_{12} exhibits three peaks in a 1 : 1 : 2 ratio reflecting effective D_{2d} solution symmetry (Fig. 5, bottom) as discussed above.[44] Interestingly, the spectra of $[Mn_{12}]^{1-}$ and $[Mn_{12}]^{2-}$ (Fig. 5, middle and top) are extremely similar to that for Mn_{12}, again exhibiting the same profile of three resonances in a 1 : 1 : 2 ratio, with only small shifts due to the differing paramagnetism of the three

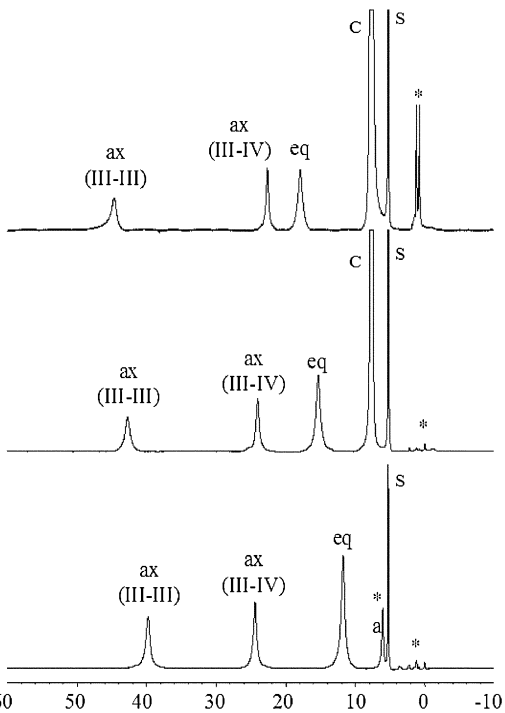

Fig. 5 ^1H NMR (300 MHz) specta at ~23 °C in CD_2Cl_2 solution of $[Mn_{12}O_{12}(O_2CCHCl_2)_{16}(H_2O)_4]$ (bottom) and corresponding $[Mn_{12}]^{1-}$ (middle) and $[Mn_{12}]^{2-}$ (top): C is $PPh_4{}^+$, * is solvent of crystallization; s is the solvent protio-impurity. Reprinted with permission from ref. 44. Copyright 2003 American Chemical Society.

complexes at 23 °C. In contrast to the low solid-state symmetry of the $[Mn_{12}]^{1-}$ and $[Mn_{12}]^{2-}$ due to their trapped added electrons, the NMR spectra indicate that, like the neutral Mn_{12}, they exhibit effective D_{2d} symmetry in solution.[15,25] Thus, not only must there be a fluxional process involving water/RCO_2^- pairs, there must clearly be detrapping of the added electrons among the outer ring of Mn atoms. In addition, this detrapping must be fast on the ^1H (and ^{19}F) NMR timescale; in fact, it is likely coupled to the H_2O/RCO_2^- fluxionality, and this is currently under detailed study by variable-temperature methods.

The described solution NMR studies probe the molecule *via* the peripheral ligation, and thus conclusions about the $[Mn_{12}O_{12}]$ core are only drawn indirectly. One way of studying the core directly is to employ ^{55}Mn NMR spectroscopy, *i.e.* directly probe the ^{55}Mn nuclei ($I = 5/2$, ~100% natural abundance). Such studies are carried out on samples in the solid state in zero applied field and at very low temperature (~2 K), and take several weeks for each good spectral acquisition.[38,39,43] Studies to date have thus been limited to complex **1** and the other high symmetry Mn_{12} complexes with R = CH_2Br and CH_2Bu^t. In accord with the S_4 symmetry of these complexes, the ^{55}Mn NMR spectra exhibit only three peaks, the four central Mn^{IV} atoms (group III), and the two sets (groups I and II) of four outer Mn^{III} atoms (Fig. 6). In addition, distinct differences are seen in the spectra from single crystals *vs.* aligned microcrystalline powder; specifically, the single crystal spectra afford significantly higher spectral resolution than the aligned powder allowing the clear observation of quadrupolar splittings on one Mn^{III} peak and the determination of quadrupole coupling parameters. A variety of other ^{55}Mn NMR studies have also been carried out, including angle-dependence studies using single crystals, and measurement of T_1 times as a function of temperature. In addition, close comparison of the spectra of **1** with those for the R = CH_2Br and CH_2Bu^t analogues has allowed a direct probe of the symmetry-lowering perturbation of the core of **1** by the hydrogen-bonding interactions with lattice $MeCO_2H$ of crystallization (*vide supra*).[39,43]

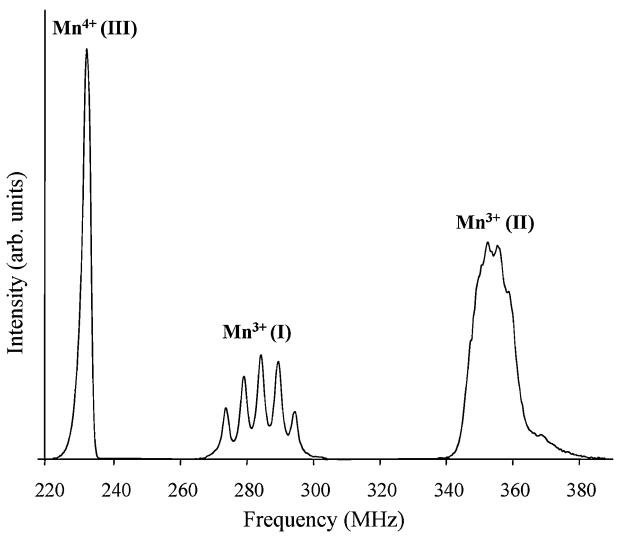

Fig. 6 ^{55}Mn NMR spectrum for a single-crystal of $[Mn_{12}O_{12}(O_2CCH_2Br)_{16}(H_2O)_4]\cdot 4CH_2Cl_2$. Numbers in parentheses refer to the group of Mn atoms, as defined in section 3.

4.3 Magnetochemistry

Direct current (dc) susceptibility studies. Variable-temperature magnetism studies have established that the Mn_{12} complexes possess $S = 10$ ground states and $D \approx -0.5\ cm^{-1}$; how these are determined is discussed below. The significant value of S can readily be rationalized on the basis of the sign and relative magnitude of the exchange interactions within the Mn_{12} core, as determined for **1** by exact diagonalization of the spin Hamiltonian, with adjustments to reproduce the bulk magnetization data:[47] the four central Mn^{IV} atoms are weakly ferromagnetically coupled (as is often the case for cubane systems owing to the acute M–(μ_3-O)–M angles), and the remaining $Mn^{III}Mn^{IV}$ and $Mn^{III}Mn^{III}$ interactions are all antiferromagnetic, with the former much stronger than the latter, as indeed is to be expected on the basis of literature data on analogous dinuclear complexes.[48] As a result, the stronger Mn^{III}–Mn^{IV} interactions overcome the weaker Mn^{III}–Mn^{III} ones within each triangular $Mn^{III}{}_2Mn^{IV}$ sub-fragment of the core, aligning the spins of the outer Mn^{III} atoms all parallel, and thus antiparallel to the central Mn^{IV} atoms (Fig. 7); this predicts an $S = 16 - 6 = 10$ ground state, as obtained experimentally by numerous studies. These spin alignments have been directly confirmed by polarized neutron scattering studies on a single crystal of $\mathbf{1}\cdot 2MeCO_2H\cdot 4H_2O$.[49] Similarly, the significant D value is primarily due to the near-parallel alignment of the eight Mn^{III} JT axes (Fig. 1, bottom); each JT distortion results in significant single-ion anisotropy for Mn^{III}, whereas Mn^{IV} and Mn^{II} are relatively isotropic. Thus, the near-parallel alignment of eight Mn^{III} JT axes leads to a significant molecular anisotropy (D value) because the latter is the tensor sum of single-ion anisotropies.

A representative plot of the magnetization (M) data for a microcrystalline powder sample of $\mathbf{1}\cdot 2MeCO_2H\cdot 4H_2O$ collected at various fields (H) and low temperatures (<10 K) is shown in Fig. 8, plotted as $M/N\mu_B$ *vs.* H/T (N is Avogadro's constant, μ_B is the Bohr magneton). For complexes populating only the ground state and possessing no axial zfs ($D = 0$), the isofield lines would all superimpose and

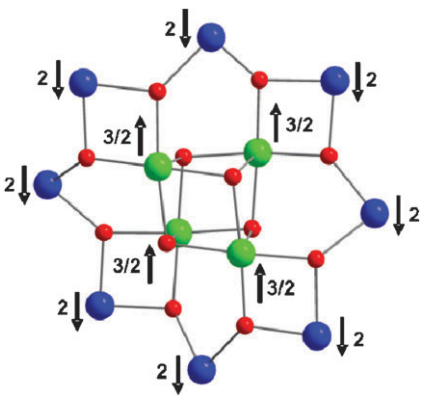

Fig. 7 Spin alignments in the ground state of Mn_{12} complexes that gives their $S = 10$ ground states. Colour scheme: Mn^{IV} green, Mn^{III} blue, O red.

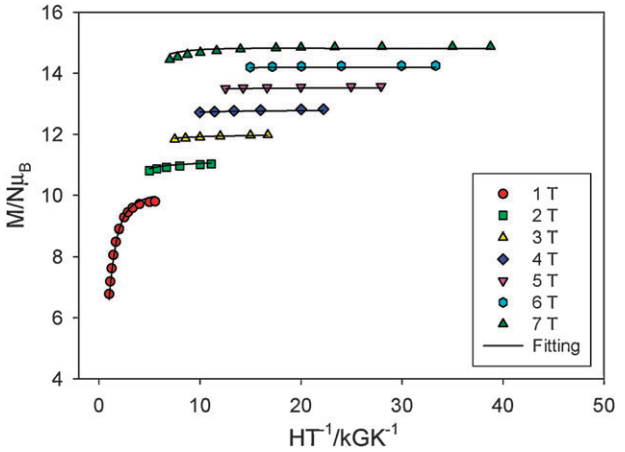

Fig. 8 Isofield plots of reduced magnetization ($M/N\mu_B$) *vs.* H/T for microcrystalline **1**·2MeCO$_2$H·4H$_2$O at the indicated fields. The solid lines show the single fit using all of the data points, employing the method described in the text.

saturate at a value of gS. However, the data in Fig. 8 clearly do not superimpose, indicating a significant D value. The data can be fit by diagonalization of the spin Hamiltonian matrix, assuming that only the ground state is populated at these temperatures (a valid assumption for normal Mn_{12} complexes), incorporating axial zfs ($D\hat{S}_z^2$) and the Zeeman term, and employing a full powder average.[50] The corresponding spin Hamiltonian ($\mathscr{H}$) is given by eqn (6), where S_z is the z-axis (the easy-axis for Mn_{12}) spin operator; the last term is the Zeeman energy associated with the applied field H. The best fit is shown as the solid lines in Fig. 8, and the fit parameters in this case were $S = 10$, $D = -0.50$ cm^{-1}, and $g \sim 2.0$. It should be added that such fits of powder magnetization data are a good but nevertheless not the best way to obtain accurate values of D and g. An alternative and particularly sensitive technique for getting accurate values of D, g and other spin Hamiltonian parameters is HFEPR spectroscopy, and many such studies have been carried out on Mn_{12} complexes to date.[38]

$$\mathscr{H} = D\hat{S}_z^2 + g\mu_B\hat{S}\cdot H \qquad (6)$$

The preparation of $[Mn_{12}]^{z-}$ (z = 1–3) derivatives has permitted assessment of the effect of changing the electron count on the resulting magnetic properties. The obtained data for the R = $CHCl_2$ complexes are summarised in Table 2.[45] The ground state S changes very little on one- and two-electron reduction, from $S = 10$ to $S = 19/2$ and back to $S = 10$, but then there is a more significant drop to $S = 17/2$ on three-electron reduction.[45] There is also an occasional report of an $S = 21/2$ ground state for some $[Mn_{12}]^{1-}$ complexes.[51] In contrast to the S value, the axial zero-field splitting parameter D does exhibit a monotonic change with the extent of reduction; there is a clear decrease in $|D|$ with progressive reduction. This is exactly as expected from the arguments above assigning the primary source of the molecular anisotropy (D value) as the eight JT-distorted Mn^{III} atoms. Since reduction involves addition of electrons onto formerly Mn^{III} atoms, converting them to Mn^{II}, the greater the extent of reduction, the fewer the remaining Mn^{III} ions and the lower the molecular anisotropy $|D|$. This argument assumes that other factors remain the same, of course, namely the overall structure of the Mn_{12} complexes and the relative orientation of the Mn^{III} JT axes essentially parallel to the molecular z-axis. This is indeed the case for $[Mn_{12}]^{1-}$ and $[Mn_{12}]^{2-}$, which have been structurally characterized. The final entries in Table 2 are the values of U, the energy barrier to magnetization relaxation. In practice, the true or effective barrier (U_{eff}) is smaller than U because the magnetization vector need not go over the top of the barrier but can tunnel through its upper regions *via* higher-lying M_S levels. This quantum tunnelling of magnetization (QTM) is a characteristic of all SMMs. Since the value of $|D|$ monotonically decreases with reduction, whereas the value of S stays roughly the same or decreases, then U decreases with reduction. The same monotonic decrease is seen for U_{eff}.[44]

Table 2 Magnetism data for $[Mn_{12}O_{12}(O_2CCHCl_2)_{16}(H_2O)_4]^{z-}$ (z = 0–3)

	$z = 0$	$z = 1$	$z = 2$	$z = 3$
S	10	19/2	10	17/2
g	1.86	1.95	1.98	1.91
D/cm^{-1}	−0.45	−0.35	−0.28	−0.24
D/K	−0.65	−0.50	−0.40	−0.34
U/K[a]	65	45	40	25

[a] Calculated as $S^2|D|$ for integer spin and $(S^2-1/4)|D|$ for half-integer spin.

A question often asked is why do the $[Mn_{12}]^{1-}$ compounds not all possess $S = 21/2$ ground states? After all, conversion of one Mn^{III} ($S = 2$) in Fig. 7 to a Mn^{II} ($S = 5/2$) should give a total $S = 16\frac{1}{2} - 6 = 21/2$. This argument, however, forgets that there are competing exchange interactions within each triangular $Mn^{III}{}_2Mn^{IV}$ sub-fragment of the Mn_{12} core, the strong $Mn^{IV}Mn^{III}$ interaction overcoming the weaker $Mn^{III}Mn^{III}$ one. On reduction to a $Mn^{II}Mn^{III}Mn^{IV}$ triangular unit, the new, weaker $Mn^{IV}Mn^{II}$ interaction is now expected to be more comparable in strength to the $Mn^{III}Mn^{II}$ interaction, and the former does not necessarily overcome the latter. As a result, the outer spins are no longer necessarily locked into being antiparallel to the central ones, with intermediate spin alignments being possible at the Mn^{II} to give an $S = 19/2$ ground state. Of course, the fact that occasionally a $[Mn_{12}]^{1-}$ complex will be found to possess an $S = 21/2$ ground state is also consistent with this picture, since it merely means that in that particular complex the $Mn^{IV}Mn^{II}$ interaction does happen to overcome the $Mn^{III}Mn^{III}$ one. It should also be noted that there is no reason to assume that adding an extra electron to one position of the molecule would not perturb the interactions at more distant parts of such a complicated system in which every metal atom is interacting with at least three others. Thus, it is perhaps not surprising that addition of a second electron to yield $[Mn_{12}]^{2-}$ now gives $S = 10$ rather than $S = 9$ or 11; again, it all depends on the exact balance of competing interactions. Similarly for $[Mn_{12}]^{3-}$.

Barrier to magnetization relaxation. Once accurate (or reasonably so) values of S and D have been obtained for a molecule, the likelihood of it exhibiting the slow magnetization relaxation of an SMM can be assessed. As stated in the

Introduction, the upper limit to the relaxation barrier (U) is given by $S^2|D|$ or $(S^2 - 1/4)|D|$ for integer and half-integer spins, respectively. As long as D is negative, then the allowed quantized orientations of the magnetization vector are as shown in Fig. 9, which is for a molecule such as Mn_{12} with $S = 10$. The $M_S = \pm 10$ pair, which are the orientations essentially on the z-axis (the quantization axis), are degenerate and at the lowest energy, and the z-axis is thus the easy-axis of magnetization. Relaxation (reorientation) of the magnetization vector from one $M_S = \pm 10$ state to another thus requires going through intermediate M_S values, and since the y-axis is energy, there is a barrier corresponding to the difference between the $M_S = 0$ and ± 10 levels. Since the relative energies of the M_S states, $E(M_S)$, for any spin S system can be calculated from eqn (7), it becomes obvious that this barrier (U) is $S^2|D|$ or $(S^2 - 1/4)|D|$ for integer and half-integer spins, respectively. In reality, the true (effective) barrier U_{eff} is usually less than U because QTM can occur through the barrier between M_S levels on one side and the other. This will be between levels of equal M_S values for the situation in Fig. 9 where there is no applied field (note that tunnelling rates are faster between higher energy M_S levels), or between levels of different M_S values at periodic applied field values when the double-well energy diagram becomes asymmetric and levels on one side are again degenerate with those on the other.

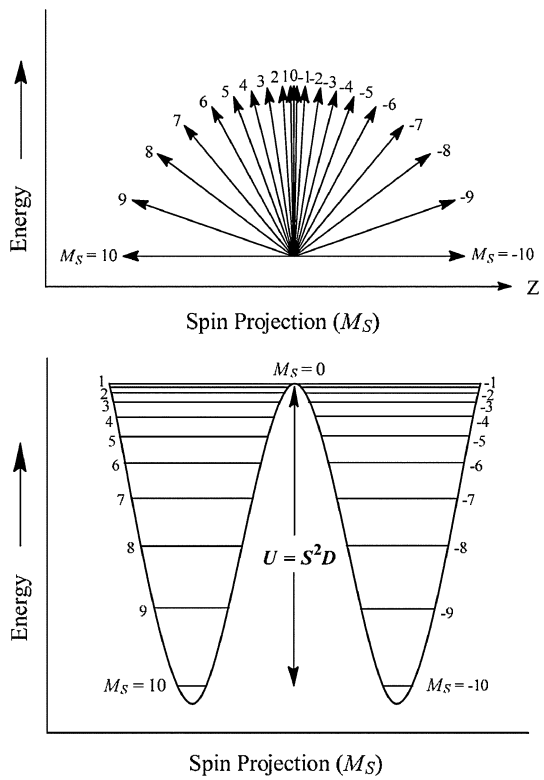

Fig. 9 (top) Plot showing the allowed, quantized orientations (M_S states) of the spin vector of a molecule such as $[Mn_{12}O_{12}(O_2CR)_{16}(H_2O)_4]$ with $S = 10$ and negative D. The relative energies of the M_S states are given by eqn (7), and thus energy increases with decreasing $|M_S|$. (bottom) An alternative figure commonly employed to depict the situation in the top figure, and indicating the barrier (U) to relaxation as being the energy difference between the $M_S = 0$ and 10 states.

A significant U_{eff} (*vs.* thermal energy kT) will thus show up as slow magnetization relaxation at an appropriately low temperature, and the molecule would then be an SMM.

$$E(M_S) = M_S{}^2D \qquad (7)$$

Alternating current (ac) susceptibility studies. On the basis of the above discussion, the most convenient way initially to determine whether a Mn_{12} (or any other compound) might be an SMM is to use ac susceptibility to probe the magnetization relaxation dynamics. In an ac susceptibility experiment, a weak field (typically 1–5 Oe) oscillating at a particular frequency (υ) is applied to a sample. The magnetization vector of the molecule oscillates in phase with the ac field, and there is thus no out-of-phase ac susceptibility signal (χ_M''), unless the temperature is lowered to a value at which the barrier becomes significant compared with thermal energy (kT). The magnetization vector cannot now stay in phase with the oscillating ac field, and a χ_M'' signal is observed, as well as a decrease in the in-phase ac susceptibility signal (χ_M'). The temperature at the χ_M'' peak maximum depends on the ac frequency (υ), increasing with increasing υ. Such a frequency-dependent χ_M'' signal is a necessary but not sufficient indicator of the superparamagnet-like properties of a single-molecule magnet. The in-phase χ_M' signal is also invaluable as an independent means to obtain the ground state S of a compound either to confirm the conclusion from the dc magnetization fit described above, or as the sole method to obtain S when dc magnetization fits are prevented by complications from the applied dc field and/or low-lying excited states (the fitting procedure assumes only the ground state is populated at all temperatures and dc fields employed).

The representative χ_M' (as $\chi_M'T$) and χ_M'' data for vacuum-dried $[Mn_{12}O_{12}(O_2CCH_2Br)_{16}(H_2O)_4]$ are shown in Fig. 10. The value of $\chi_M'T$ is ~ 50 cm^3 K mol^{-1} above ~ 9 K, which is consistent with $S = 10$ and g slightly less than 2.0, in agreement with dc fit data for this compound.[38] At lower temperatures, there is a frequency-dependent decrease in the $\chi_M'T$ and concomitant frequency-dependent increase in the χ_M'' signals. At still lower temperatures of ~ 2.5 K, there is a second feature in both $\chi_M'T$ and χ_M'', indicating the presence of a small fraction of faster-relaxing Mn_{12} species in the sample. This is characteristic of a JT isomer involving an abnormally oriented Mn^{III} JT axis (*vide supra*), which has a smaller barrier to magnetization relaxation and thus is a faster-relaxing, so-called "lower-temperature" (LT) form. Comparison of these $\chi_M'T$ and χ_M'' plots for vacuum-dried samples with those for wet (with mother liquor) samples shows that although dried samples exhibit both LT and "higher-temperature" (HT) signals, the wet samples show only the HT signal.[38] This indicates that the LT signal arises from the loss of solvent molecules and its resulting effect on the crystal lattice and Mn_{12} environments. We shall discuss the LT/HT difference further below.

Similar studies on the family of $[Mn_{12}]^{z-}$ (z = 0–3) have established that all of them exhibit the out-of-phase χ_M'' signals indicative of the slow relaxation of SMMs. For convenient comparison, we show in Fig. 11 the χ_M'' signals for $[Mn_{12}O_{12}(O_2CCHCl_2)_{16}(H_2O)_4]^{z-}$ at two ac frequencies.[45]

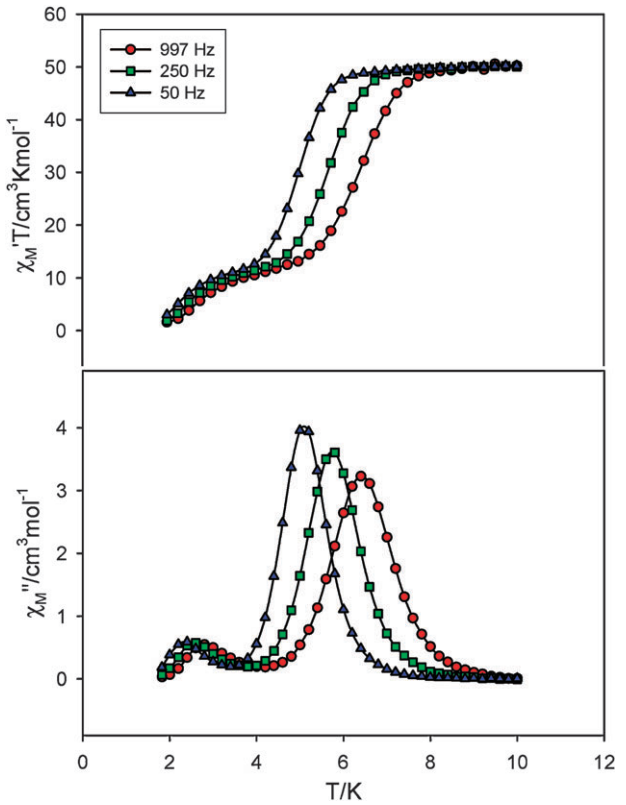

Fig. 10 In-phase χ_M' (as $\chi_M'T$) and out-of-phase χ_M'' signals for a microcrystalline sample of $[Mn_{12}O_{12}(O_2CCH_2Br)_{16}(H_2O)_4]$. Reprinted with permission from ref. 38. Copyright 2006 American Chemical Society.

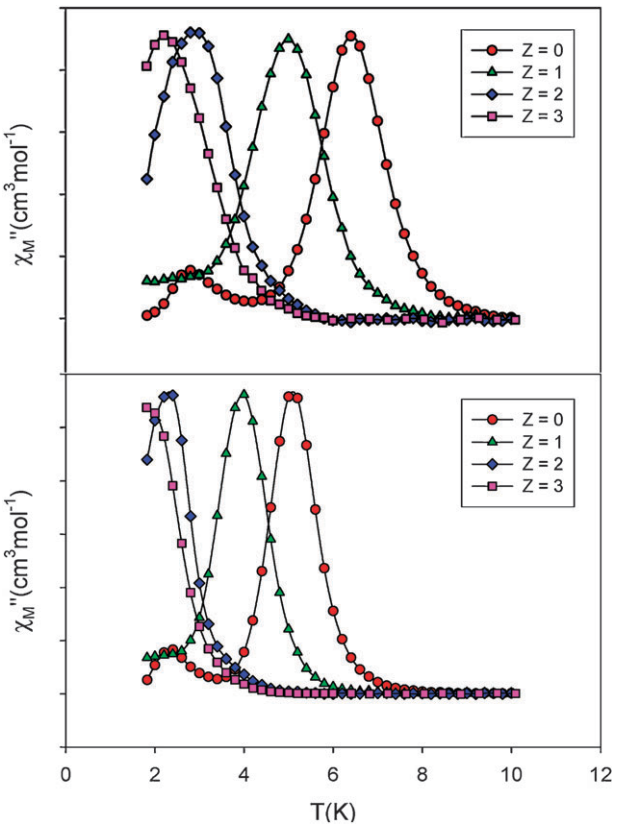

Fig. 11 Comparison of the χ_M'' *vs.* T plots for microcrystalline samples of $[Mn_{12}O_{12}(O_2CCHCl_2)_{16}(H_2O)_4]^{z-}$ (z = 0–3) at 1000 Hz (top) and 50 Hz (bottom). Reprinted with permission from ref. 45. Copyright 2007 American Chemical Society.

The peak moves progressively to lower temperature with increasing extent of reduction, consistent with a decreasing relaxation barrier as concluded from the relative values of U calculated from the S and D values in Table 2.

Ac susceptibility studies at several oscillation frequencies can be used as a means of determining the true or effective energy barrier (U_{eff}) to magnetization relaxation, because at the χ_M'' peak maximum the magnetization relaxation rate ($1/\tau$, where τ is the relaxation time) is equal to the angular frequency ($2\pi\upsilon$) of the oscillating ac field. Hence, out-of-phase ac measurements at different oscillation frequencies are a valuable source of relaxation rate *vs.* T kinetic data that can be fit to the Arrhenius equation (eqn (8)), where $\tau_0 \sim 10^{-7}$ s and $U_{eff} \sim 60$ K for **1**·2MeCO$_2$H·4H$_2$O. The value of τ_0 is about three orders of magnitude larger than usually found in superparamagnets.

$$1/\tau = (1/\tau_0)\exp(-U_{eff}/kT) \qquad (8)$$

A similar analysis allows the U_{eff} to be determined and compared for the $[Mn_{12}]^{z-}$ family, as shown for $[Mn_{12}O_{12}(O_2CC_6F_5)_{16}(H_2O)_4]^{z-}$ (z = 0–2) in Fig. 12.[15] Thus, both the shift of χ_M'' signals to lower temperatures (Fig. 11) and the observed decrease in U_{eff} value on progressive reduction (Fig. 12) reflect experimental confirmation of the faster magnetization reversal predicted from the calculated U values in Table 2, and the decreasing Mn^{III} content on reduction. Note that the value of U_{eff} depends not just on S and D but

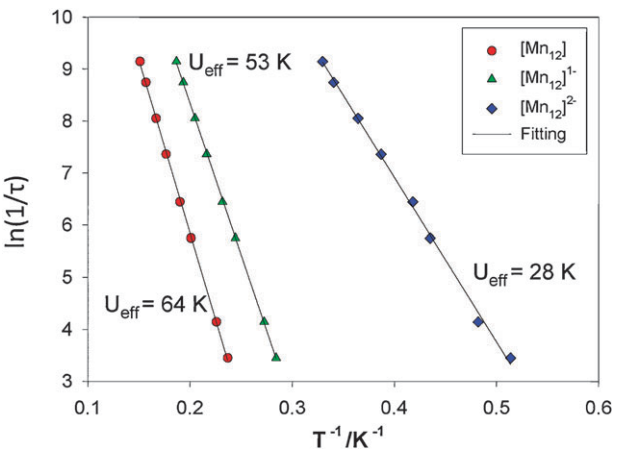

Fig. 12 Plot of the natural logarithm of relaxation rate, $\ln(1/\tau)$, *vs.* inverse temperature for $[Mn_{12}O_{12}(O_2CC_6F_5)_{16}(H_2O)_4]^{z-}$ using χ_M'' *vs.* T data at different frequencies. The solid lines are fits to the Arrhenius equation.

also on the rhombic zfs parameter E, fourth order spin Hamiltonian parameters, the precise QTM rate and pathway (*i.e.* which M_S levels of the S manifold are involved), and other parameters. These are affected by many factors including the site symmetry of the complex, and the $[Mn_{12}]^{z-}$ complexes do not all crystallize in the same space group. Thus, there are too many parameters that contribute to the observed U_{eff} to

permit a quantitative comparison between different complexes or to expect an equal decrease in U_{eff} with each reduction. The value for $[Mn_{12}]^{3-}$ is not available due to the limited χ_M'' data available above 1.8 K (the operating limit of our SQUID magnetometer) and the non-availability of single crystals for an alternative study to obtain U_{eff} using single-crystal micro-SQUID[52] methods down to 0.04 K.

Ac susceptibility measurements can also be used to investigate the nature of the magnetization relaxation processes. For a single relaxation process, as would be expected in a crystalline ensemble of molecules in identical environments with identical barriers, the χ' and χ'' behaviour as a function of angular frequency (ω), is given by eqns (9) and (10), respectively, where χ_S ($\chi_{\omega\to\infty}$) is the adiabatic susceptibility, χ_T ($\chi_{\omega\to 0}$) is the isothermal susceptibility, ω ($2\pi\upsilon$) is the angular frequency, and τ is the magnetization relaxation time. The isothermal susceptibility, χ_T, is the dc susceptibility for paramagnets obeying the Curie law. For a distribution of single relaxation processes, as would result from a distribution of molecular environments in the crystal, and a resulting range of U_{eff} barrier heights, the expressions for χ' and χ'' are now given by eqns (11) and (12), where α gauges the width of the distribution and takes values between 0 and 1.

$$\chi'(\omega) = \chi_S + \frac{(\chi_T - \chi_S)}{1 + \omega^2\tau^2} \tag{9}$$

$$\chi''(\omega) = \frac{(\chi_T - \chi_S)\omega\tau}{1 + \omega^2\tau^2} \tag{10}$$

$$\chi'(\omega) = \chi_S + \frac{(\chi_T - \chi_S)[1 + (\omega\tau)^{1-\alpha}\sin(\alpha\pi/2)]}{1 + 2(\omega\tau)^{1-\alpha}\sin(\alpha\pi/2) + (\omega\tau)^{2(1-\alpha)}} \tag{11}$$

$$\chi''(\omega) = \frac{(\chi_T - \chi_S)[(\omega\tau)^{1-\alpha}\cos(\alpha\pi/2)]}{1 + 2(\omega\tau)^{1-\alpha}\sin(\alpha\pi/2) + (\omega\tau)^{2(1-\alpha)}} \tag{12}$$

When $\alpha = 0$, eqns (11) and (12) reduce to eqns (9) and (10), respectively, describing a single relaxation process.

A means of representing such data is as a plot of χ_M' *vs.* χ_M''; this is shown in Fig. 13 and is known as a Cole–Cole or Argand plot. The symmetrical shape of the plot suggests that a single type of species is present; the dashed line is a least-squares fit of the data to a single relaxation process as described by eqns (9) and (10), whereas the solid line is a fit to a distribution of single relaxation processes as described by eqns (11) and (12). The latter fits are clearly superior and indicate a small range of molecular environments, as is typical for a molecular crystal. The α values obtained from the fits were 0.177 ($z = 0$), 0.210 ($z = 1$), and 0.126 ($z = 2$).

The magnetic properties of Mn_{12} SMMs, and indeed other SMMs, are very sensitive to their environment, surprisingly so in many cases. We have already mentioned the different hydrogen-bonding isomers in **1**·2$MeCO_2H$·4H_2O. More generally, the presence of solvent molecules and their positional or orientational variation or disorder, can lead to a significant distribution of molecular environments, contributing to a resulting distribution of D values and relaxation barriers U_{eff}, the magnitude of α, QTM step broadening in the hysteresis loops (*vide infra*), and others. It

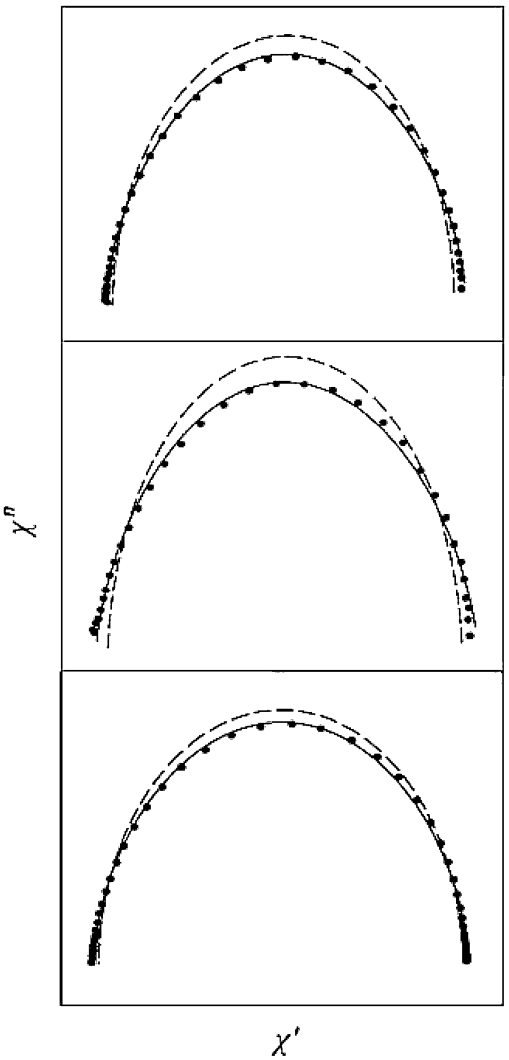

Fig. 13 Argand plots of χ' *vs.* χ'' for wet crystals of the complexes $[Mn_{12}O_{12}(O_2CC_6F_5)_{16}(H_2O)_4]^{z-}$: (top) $z = 0$ at 4.0 K, (middle) $z = 1$ at 3.4 K, and (bottom) $z = 2$ at 2.2 K. The dashed line in each case is a least-squares fit of the data to a single relaxation process as described by eqns (9) and (10). The solid line is the fit to a distribution of single relaxation processes as described by eqns (11) and (12). Reprinted with permission from ref. 15. Copyright 2005 American Chemical Society.

can even lead to completely different magnetic behaviours that can be separately studied, and two excellent examples of the latter will be described. The first is the pair of complexes mentioned earlier that are JT isomers, namely $[Mn_{12}O_{12}(O_2CCH_2Bu^t)_{16}(H_2O)_4]\cdot CH_2Cl_2\cdot MeNO_2$ and $[Mn_{12}O_{12}(O_2CCH_2Bu^t)_{16}(H_2O)_4]\cdot CH_2Cl_2\cdot MeCN$.[35] This is the case even though they crystallize in the same space group and with almost identical unit cells; in fact, the unit cell contents are essentially superimposable except that the latter has an MeCN molecule at the position of the $MeNO_2$ in the former! Their ac χ_M'' *vs.* T plots are shown in Fig. 14, and show that the isomer with the abnormal JT orientation is the LT (*i.e.* faster-relaxing) form. In accord with this, Arrhenius plots give U_{eff} values of 62 and 42 K for the HT and LT isomers, respectively. Possible origins of the faster relaxation in the LT isomer are (i) the lower symmetry core that results

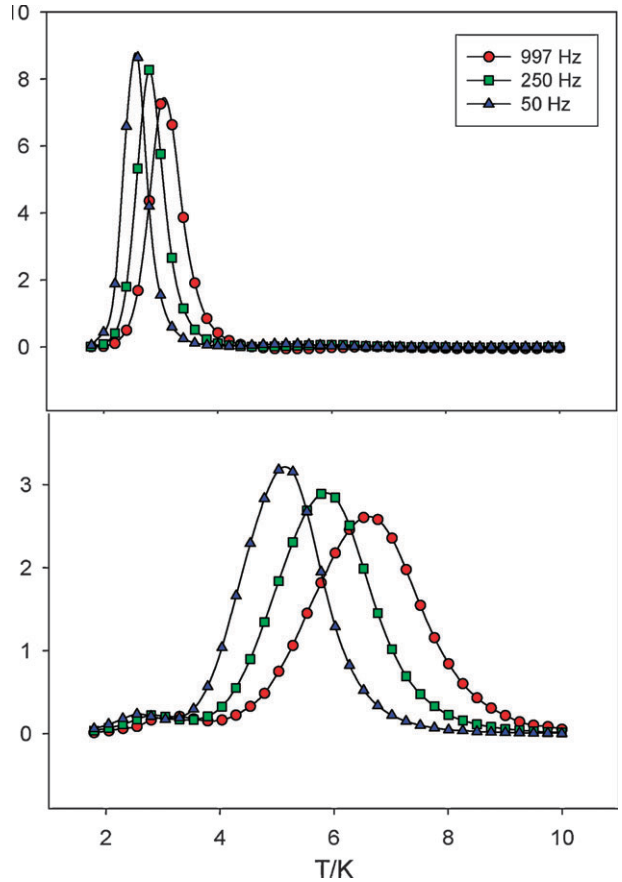

Fig. 14 χ_M'' *vs.* T plots for $[Mn_{12}O_{12}(O_2CCH_2Bu^t)_{16}(H_2O)_4]\cdot CH_2Cl_2\cdot MeNO_2$ (LT) (top) and $[Mn_{12}O_{12}(O_2CCH_2Bu^t)_{16}(H_2O)_4]\cdot CH_2Cl_2\cdot MeCN$ (HT) (bottom). Crystals wet with mother liquor and thus of undetermined mass were employed, and the *y*-axes therefore have arbitrary units.

from the abnormal JT orientation, and the faster tunnelling that consequently results from a larger rhombic (transverse) zfs parameter E; the latter mixes M_S levels on either side of the barrier and facilitates tunnelling through it; (ii) distinctly different higher-order terms in the spin Hamiltonian, which would again give different QTM rates; and/or (iii) a very low-lying excited state S manifold nesting with the ground state and providing lower-energy relaxation pathways. It should be added that detailed ^{1}H NMR, ^{2}D COSY and TOCSY spectral studies reveal that in solution there is only one species, *i.e.* JT isomerism is a solid-state phenomenon.

A second example of the importance of the solvent of crystallization is provided by the pair $(PPh_4)_2[Mn_{12}O_{12}(O_2CCHCl_2)_{16}(H_2O)_4]\cdot 4CH_2Cl_2\cdot H_2O$ and $(PPh_4)_2[Mn_{12}O_{12}(O_2CCHCl_2)_{16}(H_2O)_4]\cdot 6CH_2Cl_2$.[44] They crystallize in different space groups and have U_{eff} values of 18.5 and 30.3 K, respectively. At first, it was thought this almost factor-of-two difference was indicating JT isomerism in $[Mn_{12}]^{2-}$ complexes for the first time, but the crystal structures showed that in both cases the anions contained only normal JT orientations. Instead, the significantly different barriers must be due to the different $[Mn_{12}]^{2-}$ environments and solvent molecules, particularly the single water molecule in the former that forms a hydrogen-bond with the core, effectively lowering its symmetry.

The message that emerges from the two studies described above, and others like them, is that what are usually considered by chemists to be trivial differences that could only yield small changes to molecular properties instead result in large differences to the magnetic properties. This is another way of stating what is already common knowledge in many areas of materials nanoscience, that small changes can have big consequences at the nanoscale. In effect, one cannot say that a particular Mn_{12} (or other SMM) with particular ligands and at a particular oxidation state will have a particular barrier U_{eff}. Instead, the latter also depends significantly on subtle environmental effects such as the identity and disposition of solvents of crystallization, cations, crystal space group, local site-symmetry, and others.

Magnetization hysteresis loops. The significant Mn_{12} relaxation barriers lead to a 'freezing' of the magnetization reversal below a sufficiently low temperature, the 'blocking temperature' (T_B), which is typically in the 3–4 K region for Mn_{12} complexes. As a result, hysteresis loops are seen in magnetization *vs.* applied dc field scans.[1,52] These are best investigated on single-crystal samples using a micro-SQUID apparatus, and Fig. 15 shows the loops obtained for a single crystal of $[Mn_{12}O_{12}(O_2CC_6F_5)_{16}(H_2O)_4]\cdot 3CH_2Cl_2$, which is an SMM below $\sim$3.6 K.[15]

Several points can be made: (i) magnetization hysteresis is the diagnostic behaviour of a magnet, and is thus the ultimate proof that a molecule is an SMM, as long as one is careful to exclude the possibility of significant intermolecular interactions being present; note that one cannot completely exclude all interactions between molecules in a solid (otherwise it would be a gas) but the important thing is that they do not lead to significant magnetic interactions between the molecules, *i.e.*, they should cause no more than perturbations of single-molecule behaviour. (ii) The hysteresis loops of SMMs differ markedly from those of bulk traditional (*i.e.* 3-D) magnetic materials in exhibiting an increasing coercivity (half the loop width at $M/M_S = 0$) with decreasing temperature and with increasing field sweep rate. This behaviour is, on the other hand, that exhibited by traditional superparamagnets, *i.e.* nanoscale pieces of traditional magnetic materials with dimensions much larger than the molecular. Thus, SMMs could perhaps be better described as single-molecule superparamagnets, but traditional superparamagnets below their blocking temperature T_B are also magnets exhibiting hysteresis, so the difference is merely a matter of semantics. (iii) The loops for SMMs are not smooth but display steps due to QTM at periodic field values, *i.e.* at 0, $\sim$0.5, $\sim$1.0 T, *etc.* in Fig. 15. The steps are at field positions where M_S levels of the $S = 10$ manifold on one side of the double-well energy barrier are degenerate with M_S levels on the other side (Fig. 9), and QTM can thus occur. QTM causes an increase in the magnetization relaxation rate, giving the vertical jump (step) in the loop. The step size decreases with increasing field scan rate, as expected from the standard Landau–Zener model for tunnelling between two states.[52]

Although QTM is a characteristic property of all SMMs, and steps are essentially always seen in the hysteresis loops for

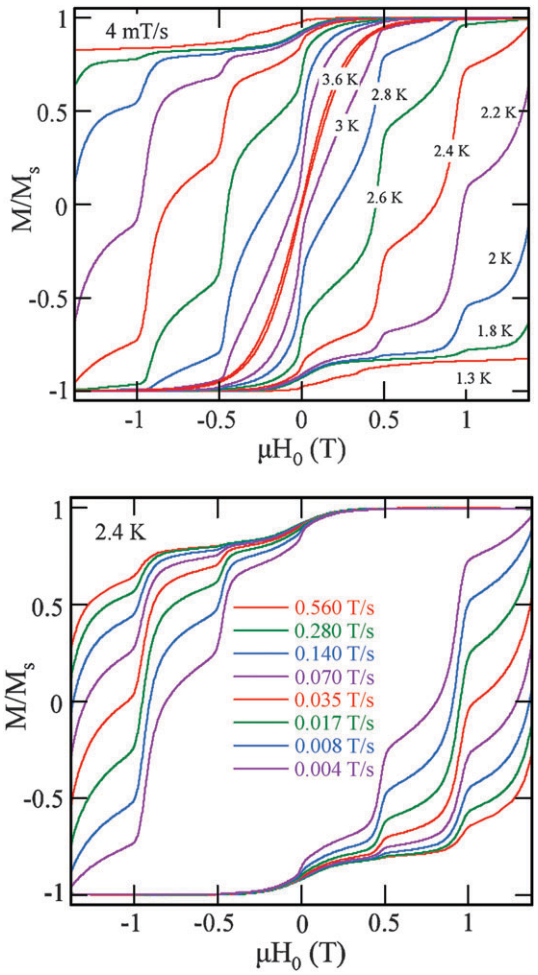

Fig. 15 Magnetization (M) hysteresis loops for a single crystal of $[Mn_{12}O_{12}(O_2CC_6F_5)_{16}(H_2O)_4]\cdot 3CH_2Cl_2$ showing the temperature dependence at a fixed sweep rate (top), and the sweep rate dependence at a fixed temperature (bottom). M is normalized to its maximum value, M_S. Reprinted with permission from ref. 15. Copyright 2005 American Chemical Society.

the Mn_{12} family, this is not always the case for other SMMs. In many cases, the steps are often broadened to the point of being smeared out, particularly for larger nuclearity SMMs. The broadening is typically due to a significant distribution of molecular environments (due to disorder in the ligands and/or in the copious solvent molecules of crystallization often present in the large voids in crystals of large molecules), which give a correspondingly significant distribution of step positions, or to a high density of low-lying excited states. The largest SMM to display QTM steps is a Mn_{22} complex,[53] although many at smaller nuclearities do not. In such cases, the presence of QTM can be established by other methods, such as a temperature-independent region at very low temperatures in the Arrhenius plot.

Hysteresis loops have also been obtained for $[Mn_{12}]^{1-}$ and $[Mn_{12}]^{2-}$ complexes, confirming them also to be SMMs. Shown in Fig. 16 are the loops exhibited by a single crystal of the $[Mn_{12}]^{2-}$ salt $(NMe_4)_2[Mn_{12}O_{12}(O_2CC_6F_5)_{16}(H_2O)_4]\cdot 6C_7H_8$.[15] Hysteresis is only observed at $\sim$1.5 K and below, in contrast to the higher temperatures for the neutral Mn_{12}

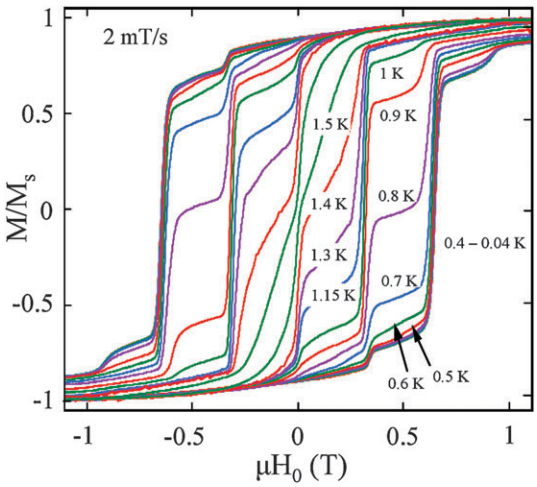

Fig. 16 Magnetization (M) hysteresis loops for a single crystal of the $[Mn_{12}]^{2-}$ salt $(NMe_4)_2[Mn_{12}O_{12}(O_2CC_6F_5)_{16}(H_2O)_4]\cdot 6C_7H_8$ showing the temperature dependence at a fixed sweep rate. M is normalized to its maximum value, M_S. Reprinted with permission from ref. 15. Copyright 2005 American Chemical Society.

complex with the same carboxylate in Fig. 15, and consistent with a significantly smaller relaxation barrier on reduction. Again, QTM steps are clearly observable at periodic values of applied field. Single crystals of $[Mn_{12}]^{3-}$ are not available for similar studies, but if they were there seems little doubt from its other properties that this oxidation state would also exhibit hysteresis loops.

When QTM steps are clearly observed in hysteresis loops, they are invaluable as a direct measure of the D value, since the field separation between the steps, ΔH, is proportional to D and given by eqn (13). In fact, this equation provides $|D|/g$, not $|D|$, but for the Mn_{12} family (and for most other Mn (and Fe) SMMs) the g value is typically $\sim$2.0 and eqn (13) thus provides a very good approximation of D for comparison with values obtained from other methods. Inspection of the steps in Fig. 15 and 16, for example, shows that those for the $[Mn_{12}]^{2-}$ complex are significantly closer together than those for the Mn_{12} complex, *i.e.* the former has a smaller $|D|$ value than the latter. This is, of course, completely consistent with the data from the other techniques discussed earlier that quantified a decreasing $|D|$ value as the Mn^{III} content of the molecules was decreased by reduction.

$$\Delta H = |D|/g\mu_B \quad (13)$$

5. Conclusions

We hope we have shown in this review how the synthetic and reactivity chemistry of the $[Mn_{12}O_{12}(O_2CR)_{16}(H_2O)_4]$ family of compounds has been developed to a very satisfying degree along many directions. This Mn_{12} family now spans four isolated oxidation states, and all four display the properties expected of an SMM. As a result, it has proven an invaluable source of comparative data on this fascinating magnetic phenomenon. It is important to emphasize that unlike many sol-gel, MOCVD and other applications of molecules in materials chemistry, SMMs are not the precursors to

interesting materials, they **are** the interesting materials, and thus retain all the advantages of molecular chemistry. In particular, the various methods that are now available for the synthesis and controlled modification of Mn_{12} molecules provide a tremendous array of related SMMs for all sorts of studies. For no other SMM type has such a large degree of controlled modification been accomplished, or a resulting large database of knowledge been accumulated, justifying our assertion that the Mn_{12} family is the *Drosophila* of single-molecule magnetism. In addition, the controlled modification has made feasible the use of Mn_{12} complexes in more intricate experiments, such as attempts to bind them to surfaces or between nano-electrodes, *etc*. It should be added that there are many interesting studies of the Mn_{12} family in the physics and related literature, of which only a very small fraction have been mentioned because they are outside the chemical scope of this Review. Nevertheless, there are probably more Mn_{12} papers in the physics than the chemistry literature, owing to the many studies of what are nanoscale magnetic particles that have become possible from the availability of crystalline, monodisperse, often identically-oriented assemblies of SMMs. Some of these can at least be mentioned for the interested reader, and selected examples include the comparative study of integer *vs*. half-integer S $[Mn_{12}]^{z-}$ complexes to probe spin parity effects in quantum tunnelling,[54] quantum phase interference in the $[Mn_{12}]^{2-}$ salts,[55] inelastic neutron scattering studies of the $[Mn_{12}]^{z-}$ (z = 0–2) family,[56] avalanche propagation (magnetic deflagration) in Mn_{12} single crystals,[57] pressure effects on QTM in Mn_{12},[58] muon spin resonance spectroscopy,[59] X-ray magnetic-circular-dichroism,[60] and many others. All these have benefitted, to some extent or other, from the simple yet powerful fact stated in the Introduction that the field of single-molecule magnetism brings all the advantages of molecular chemistry to the field of nanoscale magnetic particles. There will no doubt be many other exciting studies on the $[Mn_{12}]^{z-}$ family, and other SMMs, in the future that will also be made possible by these same advantages.

We conclude by pointing out that the very low temperatures at which the Mn_{12} compounds are SMMs (liquid He and below) mean that these molecules themselves are unlikely to ever find serious technological application. However, that does not diminish their importance. The field of superconductivity began with the discovery in 1911 of this new phenomenon in elemental mercury, and although the latter was never employed as a superconductor in a commercial device, that does not diminish the importance of mercury to that field; after all, it was the prototype of a whole new field of materials, and it provided the first example for serious study. The Mn_{12} complexes hold a similar position within the new field that has come to be known as single-molecule magnetism. It should be added, however, that there is a very big difference between superconductivity and single-molecule magnetism: there are no room temperature superconductors, which is driving the search for higher and higher T_C materials, but there are already many truly excellent room temperature magnets, some of which have been known for over two thousand years, and which are in ubiquitous use in all areas of our modern society. Whatever the future may hold for SMMs, it is unlikely that any functioning at room temperature will become available for mass use in room-temperature applications. Instead, their future is undoubtedly in low-temperature and highly specialized ones that make use of their molecular advantages of size, crystallinity, and well-defined quantum properties, and for which the expense of working at low-temperature is insignificant compared to the benefits of the application.

References

1 G. Christou, D. Gatteschi, D. N. Hendrickson and R. Sessoli, *MRS Bull.*, 2000, **25**, 66.
2 R. Sessoli, D. Gatteschi, A. Caneschi and M. A. Novak, *Nature*, 1993, **365**, 141.
3 G. Christou, *Polyhedron*, 2005, **24**, 2065.
4 D. Gatteschi, R. Sessoli and J. Villain, *Molecular Nanomagnets*, Oxford University Press, 2006.
5 J. R. Friedman, M. P. Sarachik, J. Tejada and R. Ziolo, *Phys. Rev. Lett.*, 1996, **76**, 3830.
6 L. Bogani and W. Wernsdorfer, *Nat. Mater.*, 2008, **7**, 179.
7 M. N. Leuenberger and D. Loss, *Nature*, 2001, **410**, 789.
8 G. Aromi and E. K. Brechin, *Struct. Bonding*, 2006, **122**, 1, and references therein.
9 R. Sessoli, H. L. Tsai, A. R. Schake, S. Y. Wang, J. B. Vincent, K. Folting, D. Gatteschi, G. Christou and D. N. Hendrickson, *J. Am. Chem. Soc.*, 1993, **115**, 1804.
10 T. Lis, *Acta Crystallogr., Sect. B: Struct. Sci.*, 1980, **36**, 2042.
11 H. J. Eppley, H. L. Tsai, N. Devries, K. Folting, G. Christou and D. N. Hendrickson, *J. Am. Chem. Soc.*, 1995, **117**, 301.
12 M. Burgert, S. Voss, S. Herr, M. Fonin, U. Groth and U. Ruediger, *J. Am. Chem. Soc.*, 2007, **129**, 14362, and references therein.
13 G. Q. Bian, T. Kuroda-Sowa, N. Gunjima, M. Maekawa and M. Munakata, *Inorg. Chem. Commun.*, 2005, **8**, 208.
14 S. Hill, N. Anderson, A. Wilson, S. Takahashi, K. Petukhov, N. E. Chakov, M. Murugesu, J. M. North, E. del Barco, A. D. Kent, N. S. Dalal and G. Christou, *Polyhedron*, 2005, **24**, 2284.
15 N. E. Chakov, M. Soler, W. Wernsdorfer, K. A. Abboud and G. Christou, *Inorg. Chem.*, 2005, **44**, 5304.
16 P. Gerbier, D. Ruiz-Molina, N. Domingo, D. B. Amabilino, J. Vidal-Gancedo, J. Tejada, D. N. Hendrickson and J. Veciana, *Monatsh. Chem.*, 2003, **134**, 265.
17 (*a*) E. Coronado, A. Torment-Aliaga, A. Gaita-Arino, C. Giminez-Saiz, F. M. Romero and W. Wernsdorfer, *Angew. Chem., Int. Ed.*, 2004, **43**, 6152; (*b*) D. Ruiz-Molina, M. Mas-Torrent, J. Gomez, A. I. Balana, N. Domingo, J. Tejada, M. T. Martinez, C. Rovira and J. Veciana, *Adv. Mater.*, 2003, **15**, 42.
18 C.-D. Park and D.-Y. Jung, *Bull. Korean Chem. Soc.*, 2001, **22**, 611.
19 H. H. Zhao, C. P. Berlinguette, J. Bacsa, A. V. Prosvirin, J. K. Bera, S. E. Tichy, E. J. Schelter and K. R. Dunbar, *Inorg. Chem.*, 2004, **43**, 1359.
20 G. Q. Bian, T. Kuroda-Sowa, T. Nogami, K. Sugimoto, M. Maekawa, M. Munakata, H. Miyasaka and M. Yamashita, *Bull. Chem. Soc. Jpn.*, 2005, **78**, 1032.
21 S. Willemin, B. Donnadieu, L. Lecren, B. Henner, R. Clerac, C. Guerin, A. Meyer, A. V. Pokrovskii and J. Larionova, *New J. Chem.*, 2004, **28**, 919.
22 A. Cornia, A. C. Fabretti, M. Pacchioni, L. Zobbi, D. Bonacchi, A. Caneschi, D. Gatteschi, R. Biagi, U. Del Pennino, V. De Renzi, L. Gurevich and H. S. J. Van der Zant, *Angew. Chem., Int. Ed.*, 2003, **42**, 1645.
23 M. Pacchioni, A. Cornia, A. C. Fabretti, L. Zobbi, D. Bonacchi, A. Caneschi, G. Chastanet, D. Gatteschi and R. Sessoli, *Chem. Commun.*, 2004, 2604.
24 H. B. Heersche, Z. De Groot, J. A. Folk, H. S. J. van der Zant, C. Romeike, M. R. Wegewijs, L. Zobbi, D. Barreca, E. Tondello and A. Cornia, *Phys. Rev. Lett.*, 2006, **96**, 206801.
25 P. Artus, C. Boskovic, J. Yoo, W. E. Streib, L. C. Brunel, D. N. Hendrickson and G. Christou, *Inorg. Chem.*, 2001, **40**, 4199.
26 M. Soler, P. Artus, K. Folting, J. C. Huffman, D. N. Hendrickson and G. Christou, *Inorg. Chem.*, 2001, **40**, 4902.

27 N. E. Chakov, W. Wernsdorfer, K. A. Abboud, D. N. Hendrickson and G. Christou, *Dalton Trans*., 2003, 2243.
28 C. Boskovic, M. Pink, J. C. Huffman, D. N. Hendrickson and G. Christou, *J. Am. Chem. Soc*., 2001, **123**, 9914.
29 T. Kuroda-Sowa, S. Fukuda, S. Miyoshi, M. Maekawa, M. Munakata, H. Miyasaka and M. Yamashita, *Chem. Lett*., 2002, 682.
30 T. Kuroda-Sowa, T. Handa, T. Kotera, M. Maekawa, M. Munakata, H. Miyasaka and M. Yamashita, *Chem. Lett*., 2004, **33**, 540.
31 G. Q. Bian, T. Kuroda-Sowa, H. Konaka, M. Hatano, M. Maekawa, M. Munakata, H. Miyasaka and M. Yamashita, *Inorg. Chem*., 2004, **43**, 4790.
32 S. M. J. Aubin, Z. M. Sun, H. J. Eppley, E. M. Rumberger, I. A. Guzei, K. Folting, P. K. Gantzel, A. L. Rheingold, G. Christou and D. N. Hendrickson, *Inorg. Chem*., 2001, **40**, 2127.
33 D. Ruiz, Z. M. Sun, B. Albela, K. Folting, J. Ribas, G. Christou and D. N. Hendrickson, *Angew. Chem., Int. Ed*., 1998, **37**, 300.
34 Z. M. Sun, D. Ruiz, N. R. Dilley, M. Soler, J. Ribas, K. Folting, M. B. Maple, G. Christou and D. N. Hendrickson, *Chem. Commun*., 1999, 1973.
35 M. Soler, W. Wernsdorfer, Z. M. Sun, J. C. Huffman, D. N. Hendrickson and G. Christou, *Chem. Commun*., 2003, 2672.
36 A. Cornia, R. Sessoli, L. Sorace, D. Gatteschi, A. L. Barra and C. Daiguebonne, *Phys. Rev. Lett*., 2002, **89**, 257201.
37 J. An, Z. D. Chen, X. X. Zhang, H. G. Raubenheimer, C. Esterhuysen, S. Gao and G. X. Xu, *J. Chem. Soc., Dalton Trans*., 2001, 3352.
38 N. E. Chakov, S. C. Lee, A. G. Harter, P. L. Kuhns, A. P. Reyes, S. O. Hill, N. S. Dalal, W. Wernsdorfer, K. A. Abboud and G. Christou, *J. Am. Chem. Soc*., 2006, **128**, 6975.
39 A. G. Harter, N. E. Chakov, B. Roberts, R. Achey, A. Reyes, P. Kuhns, G. Christou and N. S. Dalal, *Inorg. Chem*., 2005, **44**, 2122.
40 K. Petukhov, S. Hill, N. E. Chakov, K. A. Abboud and G. Christou, *Phys. Rev. B*, 2004, **70**, 054426.
41 S. Hill, N. Anderson, A. Wilson, S. Takahashi, N. E. Chakov, M. Murugesu, J. M. North, N. S. Dalal and G. Christou, *J. Appl. Phys*., 2005, **97**, 10M510.
42 W. Wernsdorfer, M. Murugesu and G. Christou, *Phys. Rev. Lett*., 2006, **96**, 057208.
43 A. G. Harter, C. Lampropoulos, M. Murugesu, P. Kuhns, A. Reyes, G. Christou and N. S. Dalal, *Polyhedron*, 2007, **26**, 2320.
44 M. Soler, W. Wernsdorfer, K. A. Abboud, J. C. Huffman, E. R. Davidson, D. N. Hendrickson and G. Christou, *J. Am. Chem. Soc*., 2003, **125**, 3576.
45 R. Bagai and G. Christou, *Inorg. Chem*., 2007, **46**, 10810.
46 K. Takeda and K. Awaga, *Phys. Rev. B*, 1997, **56**, 14560.
47 N. Regnault, T. Jolicoeur, R. Sessoli, D. Gatteschi and M. Verdaguer, *Phys. Rev. B*, 2002, **66**, 054409.
48 T. C. Stamatatos and G. Christou, *Philos. Trans. R. Soc. London*, 2008, **366**, 113.
49 R. A. Robinson, P. J. Brown, D. N. Argyriou, D. N. Hendrickson and S. M. J. Aubin, *J. Phys.: Condens. Matter*, 2000, **12**, 2805.
50 N. Aliaga-Alcalde, R. S. Edwards, S. O. Hill, W. Wernsdorfer, K. Folting and G. Christou, *J. Am. Chem. Soc*., 2004, **126**, 12503.
51 T. Kuroda-Sowa, M. Lam, A. L. Rheingold, C. Frommen, W. M. Reiff, M. Nakano, J. Yoo, A. L. Maniero, L. C. Brunel, G. Christou and D. N. Hendrickson, *Inorg. Chem*., 2001, **40**, 6469.
52 W. Wernsdorfer, *Adv. Chem. Phys*., 2001, **118**, 99.
53 J. T. Brockman, T. C. Stamatatos, W. Wernsdorfer, K. A. Abboud and G. Christou, *Inorg. Chem*., 2007, **46**, 9160.
54 W. Wernsdorfer, N. E. Chakov and G. Christou, *Phys. Rev. Lett*., 2005, **95**, 037203.
55 W. Wernsdorfer, M. Soler, G. Christou and D. N. Hendrickson, *J. Appl. Phys*., 2002, **91**, 7164.
56 R. Basler, A. Sieber, G. Chaboussant, H. U. Gudel, N. E. Chakov, M. Soler, G. Christou, A. Desmedt and R. Lechner, *Inorg. Chem*., 2005, **44**, 649.
57 S. McHugh, R. Jaafar, M. P. Sarachik, Y. Myasoedov, A. Finkler, H. Shtrikman, E. Zeldov, R. Bagai and G. Christou, *Phys. Rev. B*, 2007, **76**, 172410, and references therein.
58 Y. Murata, K. Takeda, T. Sekine, M. Ogata and K. Awaga, *J. Phys. Soc. Jpn*., 1998, **67**, 3014.
59 A. Lascialfari, D. Gatteschi, F. Borsa, A. Shastri, Z. H. Jang and P. Carretta, *Phys. Rev. B*, 1998, **57**, 514.
60 P. Ghigna, A. Campana, A. Lascialfari, A. Caneschi, D. Gatteschi, A. Tagliaferri and F. Borgatti, *Phys. Rev. B*, 2001, **64**, 132413.

